Synthesis of Amine-Modified Aerogel Sorbents and Metal-Organic Framework-5 (MOF-5) Membranes for Carbon Dioxide Separation

by

Teresa M. Rosa

A Thesis Presented in Partial Fulfillment
of the Requirements for the Degree
Master of Science

Approved October 2010 by the
Graduate Supervisory Committee:

Jerry Y.S. Lin, Co-Chair
Robert Pfeffer, Co-Chair
David Nielsen
Lenore Dai

ARIZONA STATE UNIVERSITY

December 2010

ABSTRACT

Amine-modified solid sorbents and membrane separation are promising technologies for separation and capture of carbon dioxide (CO_2) from combustion flue gas. Amine absorption processes are mature, but still have room for improvement. This work focused on the synthesis of amine-modified aerogels and metal-organic framework-5 (MOF-5) membranes for CO_2 separation.

A series of solid sorbents were synthesized by functionalizing amines on the surface of silica aerogels. This was done by three coating methods: physical adsorption, magnetically assisted impact coating (MAIC) and atomic layer deposition (ALD). CO_2 adsorption capacity of the sorbents was measured at room temperature in a Cahn microbalance. The sorbents synthesized by physical adsorption show the largest CO_2 adsorption capacity (1.43-1.63 mmol CO_2/g). An additional sorbent synthesized by ALD on hydrophilic aerogels at atmospheric pressures shows an adsorption capacity of 1.23 mmol CO_2/g. Studies on one amine-modified sorbent show that the powder is of agglomerate bubbling fluidization (ABF) type. The powder is difficult to fluidize and has limited bed expansion. The ultimate goal is to configure the amine modified sorbents in a micro-jet assisted gas fluidized bed to conduct adsorption studies.

MOF-5 membranes were synthesized on α-alumina supports by two methods: in situ synthesis and secondary growth synthesis. Characterization by scanning electron microscope (SEM) imaging and X-ray diffraction (XRD) show that the membranes prepared by both methods have a thickness of 14-16 μm, and a MOF-5 crystal size of 15-25 μm with no apparent orientation. Single gas

permeation results indicate that the gas transport through both membranes is determined by a combination of Knudsen diffusion and viscous flow. The contribution of viscous flow indicates that the membranes have defects.

ACKNOWLEDGEMENTS

I would like to thank my advisors, Dr. Jerry Lin and Dr. Robert Pfeffer for their understanding, guidance and thoughtful advice during my journey through the project. I would also want to thank Dr. David Nielsen and Dr. Lenore Dai for serving on my committee.

I would also like to thank my current and former labmates with whom I had the pleasure to work: Carrie, Jay, Matt, Tyler, Nick, Shriya, Haibing, Zhenxia, Chao, Xiaoli, Bo, Peter, Ding, Taylor and Stephanie. Thanks for your help, support and friendship all these years and thanks for providing a stimulating and fun environment in which to learn and grow. Carrie, I truly appreciate all your help and suggestions during the writing process of this document.

Special thanks go to Fred Peña for his invaluable help and assistance that made possible the completion of this project. Thanks for all your numerous suggestions, and for helping with all the project issues. Thanks to Marty and David, from the machine shop, for making such a beautiful job with the columns. Thanks to the CSSS staff for their tremendous help with their equipment.

I cannot finish without saying how grateful I am to my family. They have always supported and encouraged me to do the best in all areas of my life. They never let me down, and were a real support throughout all these years in school. Finally, I want to thank my soon-to-be husband, on whose constant encouragement and love I have relied throughout my time in graduate school.

Teresa

TABLE OF CONTENTS

Page

CHAPTER Page

LIST OF TABLES

TABLE Page

LIST OF FIGURES

FIGURE Page

FIGURE Page

FIGURE Page

FIGURE Page

Chapter 1

BACKGROUND

1.1 Introduction

There is a growing concern about the impact that climate change, including global warming, will have on the Earth and its inhabitants. The atmospheric levels of many greenhouse gases are increasing, including those of carbon dioxide (CO_2), which has increased by more than 30% above preindustrial levels. The vast majority of these CO_2 emissions is linked to the combustion of fossil fuels used to satisfy the escalating energy demand for electricity generation, transportation, industrial processes and other human activities (Yang et al., 2008). If no action is taken the CO_2 emissions will continue rising with the increase in consumption of fossil fuels, and will promote larger climate changes. For this reason, intensive efforts have been recently directed to reduce CO_2 emissions to the atmosphere.

Of all the strategies proposed to reduce CO_2 emissions into the atmosphere, the separation and capture of CO_2 is considered to be one of the most direct and effective approaches for achieving significant emission reductions from fossil fuel combustion sources. In fact, this approach has been identified as a high-priority research topic by several countries, including the United States. Current commercial CO_2 separation and capture technologies are very expensive and energy intensive. In these processes, CO_2 capture is the critical step because it accounts for about 70-80% of the total cost (Drage et al., 2008). This clearly indicates that the development of improved and novel technologies for CO_2

capture is necessary to achieve energy-saving and cost-effective methods of reducing CO_2 emissions into the atmosphere.

A wide range of technologies and processes have been studied for CO_2 separation and capture from flue gas streams, including: absorption in liquid sorbents, adsorption on solid sorbents, and membrane separation (Leal et al., 1995; Yang et al., 2008). Absorption in liquid amines is the most robust and widely used technology to date, which involves the use of aqueous amine solutions to remove CO_2 from gaseous streams by chemical absorption or stripping processes. This technology is energy intensive and suffers from solvent degradation and equipment corrosion problems. Adsorption on solid sorbents is based on the same principle, but uses porous solid sorbents that are surface-functionalized with amines. CO_2 is adsorbed onto the surface of the sorbent by reversible chemical bonds. In membrane separation processes porous membranes with high selectivity for CO_2 are used to separate it from other gases in a flue gas stream. These last two technologies have lower energy requirements, but still need improvement to make them cost effective for large scale applications (Yang et al., 2008). This work focuses on new research done using these two technologies.

1.2 Amine Immobilized Solid Sorbents for CO_2 Sorption

The main guideline to develop high performance solid sorbents for CO_2 separation and capture from flue gas streams is to use substrates with well-developed structural properties such as open porous structures and high surface areas for amine functionalization. An amine-functionalized sorbent should have

high CO_2 selectivity, high adsorption capacity, and ease of regeneration (Drage et al., 2008). For the solid sorbent to be economically viable and capable of providing significant energy reductions compared to the current liquid amine process, it should meet a capture capacity of 3-6 mmol of CO_2/g of sorbent (Gray et al., 2008).

1.2.1 Recent work. Research has been conducted on synthesizing amine-enriched sorbents by incorporating different amines onto the surface of porous supports such as silica gels, mesoporous silica materials, fly ash with high carbon content, and polymer substrates. One of the first reports of amine grafting onto solid sorbents for CO_2 removal was published by Leal et al. (1995). The surface of a silica gel was chemically modified with an aminosilane, and measurements of CO_2 adsorption capacity of the material were 10 cm^3 of CO_2 per gram of adsorbent (0.45 mmol/g), when exposed to a dry CO_2 environment. Later, Hiyoshi et al. (2004) studied the CO_2 adsorption capacity of SBA-15 support grafted with monoamino, diamino and triamino ethoxysilanes. The latter exhibited the highest adsorption capacity in both dry and humid streams. Huang et al. (2003) grafted 3-aminopropyltriethoxysilane (APS) on silica-based support MCM-48. The CO_2 adsorption capacity in dry atmosphere was 1.14 mmol/g, and it doubled when exposed to a humid stream. Gray's group used amine-enriched fly ash with as much as 50% carbon as a solid sorbent and reported a capture capacity of 9% of the capacity of commercially liquid amine sorbents. Recently, the same group reported CO_2 sorption on a porous poly(methyl methacrylate) (PMMA) support coated with 1,6 diazabicyclo-[5,4,0]-undec-7-ene (DBU). The CO_2 capacity of the

sorbent was 3.43 mmol/g at 298 K (Gray et al., 2008), one of the highest capacities reported so far. However, when tested at higher capture temperatures (338 K), the capacity was reduced to 2.34 mmol/g.

Although some of these sorbents exhibited respectable CO_2 adsorption capacities, there is still a need to develop more efficient solid amine sorbents that are competitive with current commercial technology. According to the literature, new solid sorbents must have CO_2 adsorption capacity of 6 mmol CO_2/g sorbent for the adsorption process to be cost-effective and more efficient than current technology (Gray et al., 2008).

1.2.2 Silica aerogels. Silica aerogels are porous solid materials that exhibit a unique combination of properties including the lowest bulk density, highest thermal insulation, and lowest optical index of refraction of any solid. They consist of fractal-like chains of molecular nanostructures each about 3-4 nm in diameter. The chains form a solid network surrounding air-filled pores of about 20 nm in diameter. Although they exhibit an extremely high porosity of 90% or greater, their structure is rigid and provides considerable mechanical strength. Due to these remarkable properties, aerogels are commercially used for several purposes such as thermal insulation material for buildings, chemical absorbent for cleaning up spills, thickening agent in paints and cosmetics, Cherenkov radiation detector, and standard media for collecting cosmic dust (Akimov, 2003; Hüsing and Schubert, 1998). In this work, silica aerogels were used as substrates to support the amines.

Silica aerogels are typically synthesized by the sol-gel method, starting with alcohol solvents and silicon alkoxide precursors such as Tetramethoxysilane (TMOS). Removal of the solvent is done by supercritical drying or by proprietary ambient pressure drying methods. The synthesis conditions of the aerogel determine the nature of its surface groups, which in turn influences the physical and chemical behavior of the aerogel (Hunt and Ayers, 2004). If the aerogel is prepared using the supercritical carbon dioxide drying process, hydroxyl (-OH) groups predominate in its surface. Therefore, the resulting aerogels are hydrophilic and degrade upon contact with water. With surface functionalization and ambient pressure drying the aerogel surface has primarily alkoxy (- OR) groups, producing hydrophobic aerogels. Figure 1.1 represents the structure of the typical hydrophilic aerogel (left) and the hydrophobic aerogel (right) after surface modification.

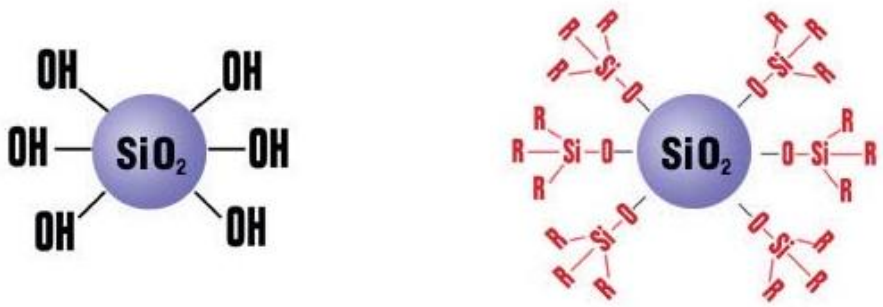

Figure 1.1. Schematic diagram of hydrophilic aerogels and hydrophobic aerogels after surface modification. R represents $–CH_3$ groups. (Cabot, 2003).

In this study, hydrophobic silica aerogels treated by Trimethylsilyl (TMS) groups followed by ambient pressure drying method were used as supports for amine-modified sorbents. The commercially produced aerogels (Nanogel ®) were

supplied by Cabot Corporation. Table 1.1 summarizes the physical properties of these Nanogels.

Table 1.1

Physical Characteristics of Cabot Nanogel Fine Particles (Cabot, 2003)

Particle Size Range	65 to 150 µm
Pore Diameter	~20 nm
Porosity	95%
Bulk Density	40 to 70 kg/m^3
Particle Density	~125 kg/m^3
Thermal Conductivity	0.018 W/m·K
Surface Area	600 to 800 m^2/g

1.3 Reactions between amines and CO_2.

Based on the studies of CO_2 absorption on aqueous amine solutions, the main pathways proposed for the reaction process between CO_2 and amines are described by pathways 1 and 2 shown below (Serna-Guerrero et al., 2008).

$$2RNH_2 + CO_2 \leftrightarrow RNHCO_2^- RNH_3^+ \quad (1)$$

$$RNH_2 + CO_2 + H_2O \leftrightarrow RNH_3^+ HCO_3^- \leftrightarrow RNH_3^+ CO_3^{2-} \quad (2)$$

In a water-free environment, primary and secondary amines (see Figure 1.2) react with CO_2 to form carbamates. However, in the presence of water CO_2 is removed by the formation of bicarbonate and, at an appropriate pH, carbonate species are also formed (Serna-Guerrero et al., 2008). As shown in Figure 1.2, tertiary amines do not have N-H bonds, which are required to form a carbamate,

so they do not react directly with CO_2. In the presence of water they promote the hydrolysis of CO_2 to form bicarbonate (pathway 2) (Rinker et al., 2000).

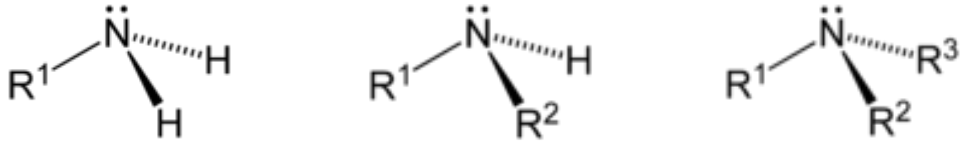

Primary amine Secondary amine Tertiary amine

Figure 1.2. Three classes of amines: primary amines have one hydrogen atom replaced by an alkyl group R; secondary amines have two atoms replaced, and tertiary have all three atoms replaced.

From pathway 1 it can be noted that the carbamate formation requires 2 moles of amines for each mol of CO_2, but for bicarbonate formation 1 mol of amines is required for each mol of CO_2 as seen in pathway 2. Therefore, the maximum absorption of CO_2 should be achieved when all the CO_2 is converted to bicarbonate (Hook, 1997). Although the production of carbamate is faster than the production of bicarbonate, in the first pathway the absorption of CO_2 is limited by its stoichiometry. In the second pathway the absorption of CO_2 is limited by the slow kinetics (Serna-Guerrero et al., 2008).

It is thought that the same reactions occur between CO_2 and the functionalized amines on the surface of a solid sorbent such as silica aerogels. However, the reaction mechanism in this case may be more complicated with the presence of physical adsorption (Serna-Guerrero et al., 2008).

1.4 Gas Fluidization.

1.4.1 General characteristics of fluidized beds. In gas fluidization, a gas is passed upwards through a bed of solid particles at velocities that cause the particle-gas mixture to behave as a fluid. Fluidized beds are widely used in industry for dispersing solid particles in a gas stream for applications such as coating, granulation, adsorption and desorption, blending and mixing, and drying. Fluidized beds are also used in processes where catalysts or sorbents require continuous regeneration. The attractiveness of using gas fluidization in these industrial processes stems from its capability of continuous powder handling, high levels of intermixing, high contact area between fluid and solid, and high rates of heat and mass transfer (Geldart, 1990; Quevedo et al., 2010).

The behavior of particles in a fluidized bed depends on properties such as size and density. Geldart classified the fluidization of particles into four groups that are shown in Figure 1.3 (Geldart, 1990). Powders in group A are easily fluidized with smooth fluidization at low gas velocities and controlled gas bubbles that break down at high velocities. The bed takes long time to de-aerate after the gas stops flowing. Group B are sand-like powders that fluidize with intense bubbling due to the absence of interparticle forces. The bed collapses instantly after the gas flow is interrupted. Group C consists of cohesive, very fine powders that are difficult to fluidize because the interparticle forces –e.g. van der Waals and electrostatics– are greater than those exerted by the fluidized gas. As a result, the gas flows through channels and cracks within the powder. Group D are large, dense particles that spout from the top of the bed easily. Bubbles coalesce and rise

slower than the rest of the gas, and slugs are formed when the bubble size is similar to the bed diameter. Like with Group B, the bed collapses instantaneously when the gas stops flowing.

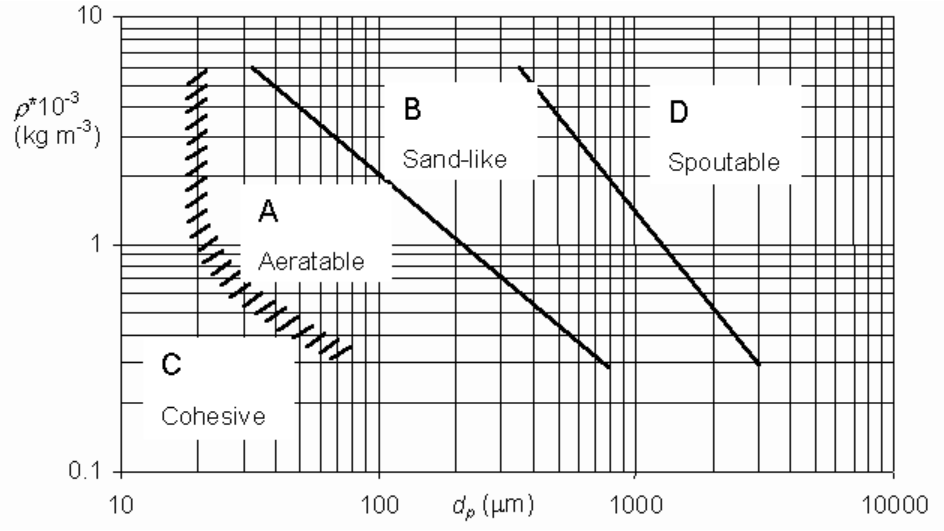

Figure 1.3. Geldart classification of powders according to fluidization properties at air ambient conditions (Kunii and Levenspiel, 1991).

The hydrodynamic characteristics and fluidization behavior of nano-powders and nanostructured powders such as aerogels are quite different from any of the powders classified under the Geldart criteria. Because of the high cohesive forces between the particles, nanopowders tend to form large stable agglomerates, and it is these agglomerates that are fluidized, rather than the individual particles. However, given their small size and extensive surface area, many nanostructured powders will only fluidize at high superficial velocity, accompanied by vigorous bubbling and powder elutriation.

1.4.2 Assisted fluidization by a micro-jet. Because of their strong interparticle forces, nanostructured particles such as aerogels tend to form larger-sized agglomerates. Some nanoparticles, such as hydrophobic silica nanopowders fluidize smoothly at low minimum fluidization velocity, and have high bed expansions with almost no bubbles, somewhat similar to Geldart Group A. This type of fluidization of nanoparticle is called agglomerate particulate fluidization (APF) and has been extensively studied by Zhu et al. (2005). Other types of nanopowders, such as hydrophilic silica and titania, require much higher minimum fluidization velocities, have limited bed expansion, and gas bypassing due to rising large bubbles and elutriation of particles is significant. This fluidization behavior is called agglomerate bubbling fluidization (ABF), somewhat akin to Geldart Group B.

To overcome the problems of fluidizing ABF type nanoparticles, a high pressure secondary gas flow through a micro-jet can be added to the bed. This additional high-velocity (sonic) flow produces high shear and turbulence in the vicinity of the jet and breaks up large agglomerates into much smaller particle agglomerates, thereby significantly reducing the minimum fluidization velocity, and eliminating bubbling and elutriation (Quevedo et al., 2010; Pfeffer, et al., 2007).

1.4.3 Hydrodynamic characteristics. The fluidization quality of a fluidized bed can be determined by measuring the pressure drop and the expansion of the bed with changes in gas velocity. Figure 1.4 shows the typical plot of pressure drop as function of gas velocity. When there is no flow the

pressure drop is zero and the bed height is the initial height. As the gas velocity increases, the pressure drop gradually increases while the bed height remains fixed. In this region the bed behaves as a packed bed. At the minimum fluidization velocity, U_{mf}, the upward force exerted by the gas balances with the weight of the particles and the particles start to float in the gas. At this point the bed starts expanding in height and the pressure drop starts to plateau because of the force balance. If the gas velocity is increased further, the bed continues to expand and the pressure drop stays constant.

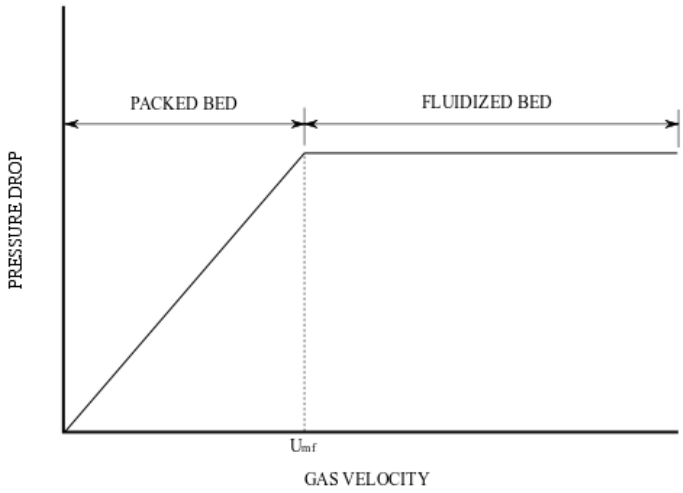

Figure 1.4. Diagram of pressure drop as function of gas velocity.

The pressure drop at the plateau can be calculated by simply dividing the initial weight of the bed by the cross-sectional area of the column as shown in Equation 3.

$$\Delta p = \frac{M_B g}{A} \tag{3}$$

where Δp is the pressure drop of the bed, M_B is the total mass of the particles, g is the gravity constant, and A is the cross-sectional area of the column.

This equation assumes that the density of the gas (buoyancy) is much smaller than the density of the particles, all of the particles participate in the fluidization (none stick to the walls of the column), and wall friction are negligible.

1.5 Membrane separation

The development and fabrication of ordered porous materials such as zeolites and mesoporous silica in the form of membranes has had significant progress in gas separation and storage applications. Although most of these inorganic membranes have shown better performance than polymeric membranes, they are still limited by the difficulties in varying pore size and functionalizing groups. These difficulties may be overcome by metal-organic frameworks (MOFs), which are a relatively new class of crystalline porous materials that show promise for CO_2 separation applications. Their structural combination of inorganic metal clusters and organic ligands offers unique properties such as tunable pore size, large surface areas and pore volumes, and great design flexibility (Gascon and Kapteijn, 2010). These properties offer new opportunities for potential superior performance.

1.5.1 Metal-organic framework (MOF-5). Also known as isoreticular metal-organic framework-1 (IRMOF-1), MOF-5 is the simplest and most well-studied MOF. As illustrated in Figure 1.5 the structure of MOF-5 consists of clusters or units of $Zn_4O(CO_2)_6$ that are joined together by benzene links. Each individual unit is composed of four ZnO_4 tetrahedra (blue) with a common vertex and six carboxylate C atoms that form the octahedral unit. This forms a three dimensional cubic framework with the octahedral units at its vertices and the

benzene links as the edges (Yaghi, et al., 2003). This open framework leads to some exceptional properties (listed in Table 1.2) that have increased the interest in studying this new material for potential applications on gas adsorption, separation and storage. One method that has been studied recently is to prepare MOF-5 membranes that could be used for gas separation as storage such as CO_2.

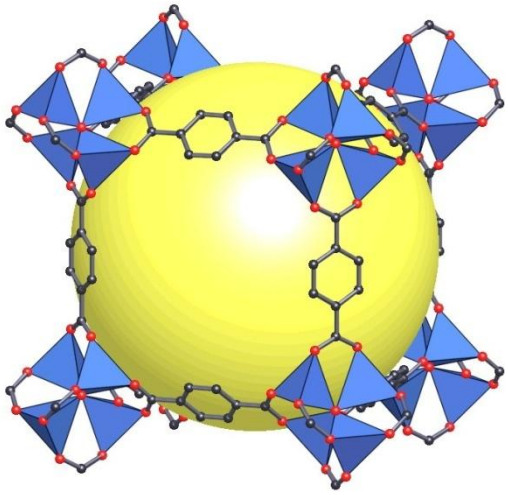

Figure 1.5. Illustration of the MOF-5 framework. The unit cell is formed by eight $Zn_4(O)(BDC)_3$ clusters that enclose a large cavity shown by the yellow sphere (Li et al., 1999).

Table 1.2

MOF-5 Properties (Li et al., 1999)

Langmuir surface area	2900 m^2 g^{-1}
Density	0.59 g cm^{-3}
Micropore volume	0.61-0.54
Pore aperture width	8 Å
Pore diameter	12 Å
Thermal stability	300°C

1.5.2 Synthesis of MOF-5 membranes. The formation of a MOF-5 membrane requires the development of a continuous, defect-free layer of MOF-5 crystals, so that gas transport takes place only through the crystals pores. To accomplish this, MOF-5 crystals are deposited on the surface of a porous support which provides mechanical strength and allows the growth of a uniform structure. This is analogous to the synthesis of zeolite membranes, where crystals are slowly grown from a solution of metal precursor and bridging ligands by using a hydrothermal route. The two most common hydrothermal synthesis methods used to prepare MOF-5 membranes are: in situ synthesis and secondary growth (ex situ) synthesis.

1.5.2.1 In situ hydrothermal synthesis method. This is a simple and direct method in which nucleation, deposition and crystal growth occur simultaneously. Basically, the porous support is immersed into a precursor solution and the MOF-5 membrane is synthesized under autogenous pressure in an autoclave for a specific temperature and duration. The precursor solution contains zinc nitrate, terephthalic acid, which provides the organic ligand, and an organic solvent. After the synthesis is completed, a thin layer of MOF-5 crystals is formed on top of the porous support (Mallada and Menéndez, 2008; Pabby et al., 2009).

The formation of a continuous membrane depends on experimental conditions including composition of the precursor solution, support material, and how the support is in contact with the solution. It is also sensitive to synthesis conditions such as temperature, precursor concentration, and duration (Lin, et al., 2002).

Because the nucleation and crystallization take place at the same time, the membrane will be formed of multiple layers of randomly oriented crystals, resulting in intercrystalline gaps. To minimize defects, post treatment can be done by growing additional membrane layers (O'Brien, 2009).

Few reports on the synthesis of MOF-5 membranes by in situ method on different supports have been published. Hermes et al. (2005) reported the selective nucleation and growth of MOF-5 thin films on silica and alumina surfaces with self-assembled monolayers. More recently, Liu et al. (2009) reported the synthesis of continuous MOF-5 membranes on porous α-alumina supports.

1.5.2.2 Secondary growth hydrothermal synthesis method. In this method the nucleation, deposition and crystal growth processes are separated in two steps. In the first step nucleation and initial crystal growth are carried out in a primary precursor solution to yield MOF-5 crystals. Then, the crystals are used as seeds that are deposited on the surface of the porous support by deep coating it in a suspension. In the second step, the seeded support is brought into contact with a secondary precursor solution where further growth of crystals occurs under hydrothermal synthesis conditions. The concentration needed for the secondary growth is lower than that required for the nucleation step, so almost all of the crystals grow over the existing seeds. By controlling the composition and concentration of the secondary solution, the rate and orientation of the crystals can be controlled (Mallada and Menéndez, 2008; Pabby et al., 2009). Compared to the in situ method, secondary growth synthesis requires lower temperatures and

shorter synthesis time. Also, the seed layer allows easier coverage of crystal layer (Lin, et al., 2002).

Reports of synthesis of MOF-5 membranes by secondary growth method include Yoo and Jeong (2008) who synthesized MOF-5 layers on a porous alumina substrate that had been previously coated with a conductive layer, and Ranjan and Tsapatsis (2009) who reported the synthesis of microporous MOF on porous alumina supports.

Despite the increasing interest in preparing MOF-5 membranes, the synthesis of a continuous, uniform and defect-free membrane is still a challenge and is not well understood.

1.6 Research Objectives and Structure of Thesis

As mentioned above, current commercial processes to separate and capture CO_2 from coal-fired combustion streams are expensive and energy intensive. CO_2 capture is the critical step as it is estimated to represent three-fourths of the total cost of a carbon capture, storage, transport, and sequestration system. Therefore it is imperative to develop improved and more efficient processes or technologies that achieve significant reduction of CO_2 emissions to the atmosphere. Two technologies that have gained increasing attention due to their lower energy requirements are adsorption of CO_2 by solid amine sorbents and membrane separation.

At the present stage, numerous studies of CO_2 adsorbents prepared by functionalizing amines on the surface of different solid supports have been reported, but they still have relatively poor performance when compared to

existing sorbents. The unique properties of silica aerogels -i.e. very large porosity and surface area per unit mass- make them attractive to be used as supports for immobilized amines making an efficient CO_2 adsorbent. However, no work has been reported on using aerogels as supports for a sorbent for CO_2 capture.

Membrane separation processes provide several advantages over other separation techniques, including energy efficiency and easiness of use. However, the membrane processes reported in literature to date do not exhibit the high flux, selectivity and stability necessary to make them a viable process. The large porosity and adjustable chemical functionality of MOF-5 membranes make them promising to capture CO_2 from flue gases. However, the preparation of MOF-5 thin films remains a challenge due to the difficulties in controlling synthesis conditions.

This thesis presents early stage research on two new ideas for improving the performance of these two technologies for CO_2 capture: synthesis of amine functionalized aerogels and synthesis of MOF-5 membranes. The objectives for the synthesis of amine functionalized aerogels are:

(1) To synthesize amine coated nanostructured silica aerogels and to study the CO_2 adsorption properties of these sorbents using mixtures of CO_2 and N_2 to simulate a flue gas stream.

(2) To study the hydrodynamic characteristics of the amine modified aerogels configured in a microjet-assisted gas fluidized bed.

The objectives for the synthesis of MOF-5 membranes are:

(1) To synthesize and characterize MOF-5 membranes by two methods: in situ and secondary (seeded) growth.

(2) To compare the characteristics and morphology of MOF-5 membranes prepared by both synthesis methods.

This thesis consists of two parts. Chapter 2 focuses on the synthesis of amine functionalized aerogels by various methods to coat the amines. Results of CO_2 adsorption capacity and fluidization behavior of the aerogels are also presented. Chapter 3 focuses on the synthesis of MOF-5 membranes on α-alumina supports via in situ and secondary growth methods. Characterization and comparison of each membrane is discussed. Finally, Chapter 4 presents conclusions and recommendations for future work.

Chapter 2

AMINE-FUNCTIONALIZED AEROGELS

2.1 Introduction

As mentioned in Chapter 1, functionalizing amines on the surface of silica aerogels can potentially result in a high performance sorbent for CO_2 capture. This chapter explores three methods of immobilizing the amines onto the aerogels surface: physical immobilization, magnetically assisted impact coating (MAIC) and atomic layer deposition (ALD). The adsorption capacity of the amine-modified sorbents is described and discussed. Also, the hydrodynamic characteristics of the fluidized bed of one of the samples are presented.

It is necessary to present a brief background of the synthesis methods before presenting the work done. The physical immobilization method is the simplest, and consists of the direct mixing of the amines and substrates in water with the assistance of a tumbler mixer. This results in the physical adsorption of the amines on the support surface. The following subsections provide a background of the more complex methods of MAIC and ALD.

2.1.1 Magnetically assisted impact coating (MAIC). MAIC process is a dry coating technique used to synthesize particulates with controlled surface coatings. This process has been successfully used to coat sub-micron guest particles onto larger host particles to create composite particles with different surface properties. Magnetic particles made from barium ferrite coated with polyurethane are used to assist in the coating process. In MAIC, a hollow cylindrical chamber is filled with the magnetic, host and guest particles, and is

placed in an alternating magnetic field (see Figure 2.1). In the presence of the magnetic field, the magnetic particles accelerate and rotate causing random collisions with each other, with other particles and with the walls of the chamber. The fluidized motion of the particles causes the guest particles to be uniformly coated onto the host particles by means of particle impaction. The resulting coating of the guest particles depends on various operating conditions including processing time, weight fraction and size ratio of guest to host particles and particles properties (Ata et al., 1998; Ramlakhan et al., 2000; Yang et al., 2005).

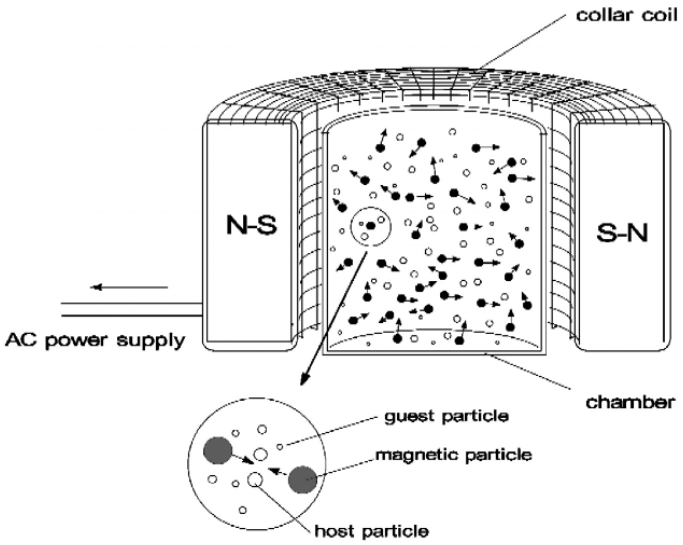

Figure 2.1. Schematic diagram of the batch MAIC device (Ramlakhan et al., 2000).

The guest particles can be substituted by liquid to apply liquid coatings to solid particulate substrates. In this case, it is required that the liquid and the solid particulate have some affinity or wetting ability. The physical forces operating within the system assure that the liquid is film-coated onto the host particles. Various liquids have been successfully coated onto particulate substrates.

For example, Hendrickson et al. (1998) have coated nano-silica and nano-titania substrates with different coupling agents such as ambifunctional and polyfunctional silanes.

2.1.2 Atomic layer deposition (ALD). Atomic layer deposition (ALD) is a gas phase coating technique that uses alternate surface reactions to deposit thin films on substrates. ALD is similar to the chemical vapor deposition (CVD) process, except that in ALD a binary reaction is split into two half-reactions. By using sequential surface reactions this technique provides deposition of conformal thin-films with atomic level control.

As illustrated in Figure 2.2, film growth occurs in a cyclic manner. Initially, the first precursor is pulsed and reacts with the exposed surface of the substrate, forming an atomic monolayer on the surface. Then, any excess precursor and byproducts are purged or evacuated. Next, the second precursor is pulsed and reacts with the surface to form another layer on top of the first layer. Again, all excess precursor and byproducts are purged or evacuated. The cycle is repeated alternating the half reactions until the required thickness is achieved. Ideally, during each reaction the reactants saturate completely the active sites on the substrate surface, making the process self-limiting and self-controlling (Ferguson et al., 2002; Ritala and Leskelä, 2002).

ALD has been used in the synthesis of monolayer catalysts and gas sensors based on nanoporous materials with high surface areas and low densities. Published literature shows reports of successful use of ALD to coat zinc oxide (ZnO), tungsten (W), titanium dioxide (TiO_2) and alumina (Al_2O_3) on the inner

surface of silica and carbon aerogels (Kucheyev, et al., 2005; Baumann et al., 2006; Ghosal et al., 2009; Hakim et al., 2005).

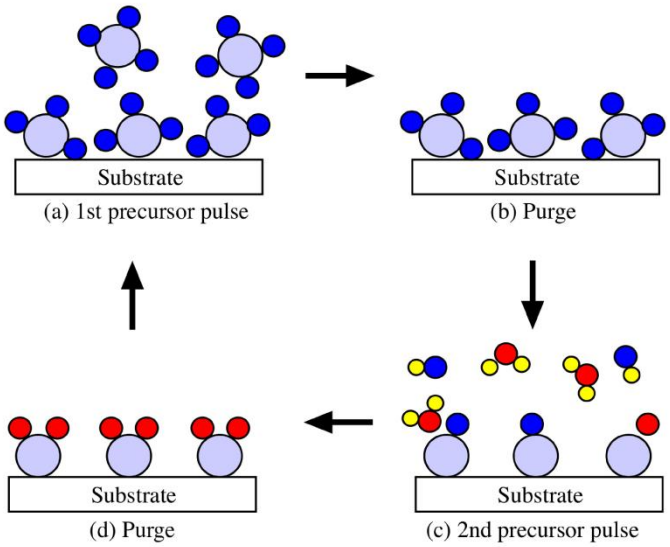

Figure 2.2. Illustration of ALD process based on alternate surface reactions (Barron, 2009).

2.2 Experimental

2.2.1 Synthesis of amine functionalized aerogels. Four organic compounds containing one, two or three amino groups were selected to functionalize the surface of the aerogels, and a summary of their properties is shown in Table 2.1. Triameen T, Duomeen T and γ-APS were chosen because of their multiple primary and secondary amino groups. PEI has been effectively used before to synthesize CO_2 adsorbents by impregnation on several mesoporous silica nanoparticles such as SBA-15 and MCM-41. Figure 2.3 lists the amines that were used in each synthesis method.

Table 2.1

Physical/Chemical Characteristics of Amine Compounds Selected for Modification of Aerogel Surface

Abbreviation	Triameen T	Duomeen T	γ-APS	PEI
Full name	N-tallow alkyl dipropylene triamine	N-tallow alkyl trimethylene diamine	3-aminopropyl triethoxysilane	Poly-ethyleneimine
Chemical formula	R-NH-$(CH_2)_3$-NH-$(CH_2)_3$-NH_2	R-NH-$(CH_2)_3$ -NH_2	H_2N-$(CH_2)_3$ -Si-$(OC_2H_5)_3$	$(CH_2CH_2NH)_n$
Boiling point (°C)	>150	>300	217	not available
Melting point (°C)	40	44	-70	73-75
Density (g/cm^3)	0.845	0.821	0.949	1.01
Viscosity (Cp)	17	8	not available	not available

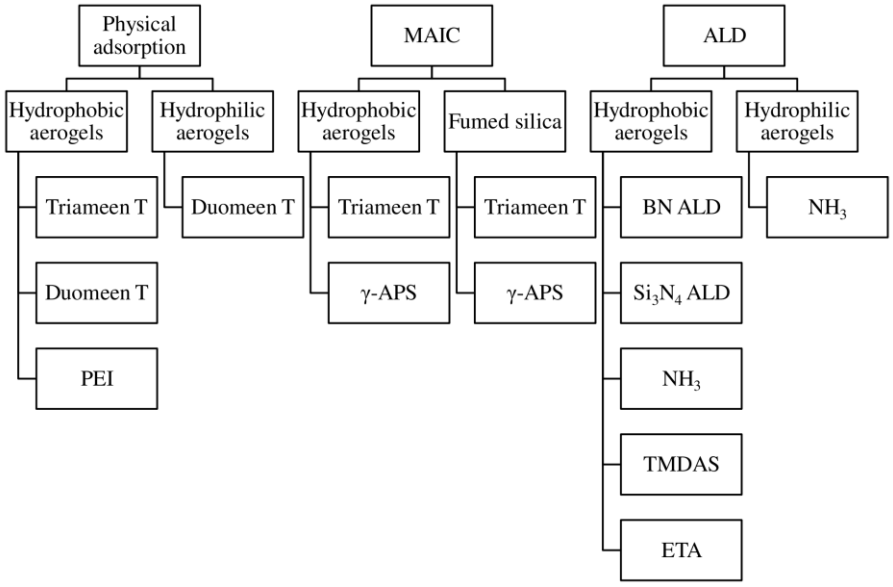

Figure 2.3. Schematic of amines used in each synthesis method.

2.2.1.1 Physical adsorption of amines on aerogels. Four amine surface-modified aerogels were prepared with Triameen T, Duomeen T and PEI as the amine sources. The amines were dissolved in water using a ball mill type tumbling mixer. Then, the aerogels were added to the amine solution and mixed until they were no longer floating on the surface. Because the aerogels are hydrophobic, it was assumed that all the amines had entered the pores and adsorbed on the aerogel granules when they stopped floating on water. After complete mixing was achieved, the resulting slurry was filtered with vacuum and dried at 100 °C overnight. The proportion of amine to aerogel for all samples was 1.5:1 by weight. Hydrophobic aerogels (Cabot Nanogel TLD 203) having a size range of 65-150 μm, were used for all samples, and an additional sample was prepared with hydrophilic aerogels (oxidized Nanogel) and Duomeen T. (See Appendix B.1).

2.2.1.2 Amine coated aerogels by MAIC batch process. Samples synthesized by this method were prepared by AVEKA, Inc., the company that patented the MAIC process. Triameen T and γ-APS were coated on two supports: hydrophobic silica aerogels and fumed silica nanoparticles (trade name Aerosil 200). The latter is a hydrophilic fumed silica nanopowder with an average particle size of 12 nm and a surface area of 200 ± 25 m^2/g. Both amine surfactants were diluted in water (25 wt%) to lower their viscosity, so they could be spread over the aerogels in the MAIC process. A weighed amount of aerogel particles (host particles) and diluted surfactant were added to the processing vessel. A measured mass of magnetic particles was also placed in the vessel. An oscillating external

magnetic field was created by using coils powered by AC surrounding the vessel, and the particles were mixed for 10 minutes. Finally, the resulting wet powder was dried at 100 °C overnight.

2.2.1.3 Amine coated aerogels by ALD. Samples modified with ALD were prepared by Dr. David King from the University of Colorado at Boulder, Colorado. Two ALD schemes of metal nitrides were used to coat amines on the aerogel surface: boron nitride (BN) ALD and silicon nitride (Si_3N_4) ALD. In addition, surface functionalization of the aerogels with no ALD was done with ammonia (NH_3), Tris-dimethylamino-silane (TDMAS) and ethanolamine (ETA). The samples were prepared in a fluidized bed of aerogels in vacuum at different temperatures ranges between 23 to 500 °C. One sample was prepared with hydrophilic aerogels at atmospheric pressures. For hydrophobic aerogels each ALD cycle was started with the second half of the cycle (second precursor) before doing one full cycle because of the tri-methyl-silyl (TMS) groups already on their surface.

2.2.2 TGA-DSC measurements. Simultaneous thermal gravimetric analysis and differential scanning calorimetry (TGA-DSC) measurements conducted by a TA Instrument SDT Q-600 system were used to calculate the amount of amine coated on two modified aerogel samples. During the analysis samples of about 18 mg of aerogels modified with Triameen T and Duomeen T were loaded in the sample holder and were heated from 25 °C to 700 °C in a nitrogen atmosphere at a constant rate of 3 °C/min. Changes in weight and heat as function of temperature were recorded to detect any amine decomposition or

phase transition. TGA-DSC measurements were also conducted on unmodified hydrophobic and hydrophilic aerogels to use as a control.

2.2.3 Carbon dioxide adsorption using Cahn microbalance. Room temperature adsorption measurements were conducted as described in (Zhao et al.; 2009) on a Cahn electronic microbalance system (Cahn D-101) as shown in Figure 2.3. A stainless steel sample pan was suspended with a platinum wire (Gauge 36, Fisher Scientific) from one arm of the balance. The pan was enclosed in a quartz tube. Pure CO_2 and mixtures of CO_2 and nitrogen were used as sorption gas to simulate a flue gas stream. An additional stream of pure nitrogen was used as the purge gas.

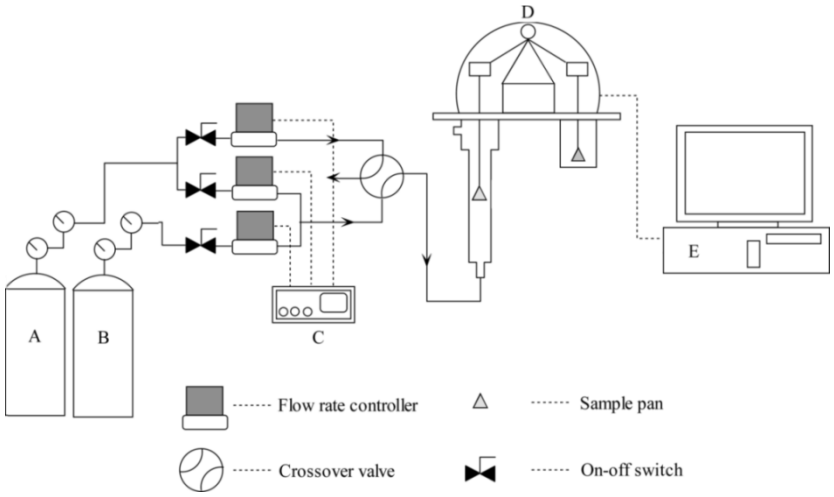

Figure 2.4. Diagram of Cahn microbalance system for CO_2 adsorption studies. (A) CO_2, (B) Nitrogen, (C) flow rate readout, (D) microbalance, (E) computer (Zhao et al.; 2009).

When needed, water vapor was added to the system by flowing the gas through a cold trap with water. After the gas was saturated with vapor, it was sent to the sample inside the tube. All gases were delivered to the system by switching of a

crossover valve (Swagelok). Weight changes of the sample were recorded by a computer-aided data acquisition system.

Approximately 10 mg of degassed aerogel samples were weighed in the stainless steel pan under nitrogen flow at 100 mL/min. After the sample weight became constant, the adsorption process was initiated by switching from purge gas to sorption gas at 100 mL/min and run until the weight became constant. The weight gain as a function of time was used to calculate the CO_2 uptake (mmol gas adsorbed / g of adsorbent). Initially, adsorption of pure CO_2 was measured for each amine-modified aerogel sample, and the one that had the highest adsorption was tested again with a CO_2 concentration similar to that of a flue gas stream (~12%$_v$).

2.2.4 Fluidization experiments with aerogels. The fluidization behavior of several unmodified and modified aerogel samples was tested in a fluidized bed setup similar to the one illustrated in Figure 2.4. Two fluidization columns –1 inch and 3 inch diameter- made of cast acrylic plastic were used in the same setup. Two lines of dry nitrogen were used as fluidizing gas, one at low pressure of 20 psig and the other one at medium pressure of 120 psig. The low pressure line was introduced through a distributor plate at the bottom of the column. Using a needle valve, part of this flow was bubbled through a tank containing ethanol or a solution of ethanol and water to add alcohol vapor to the dry gas. This vapor was used to reduce the electrostatic charge effects generated by entrained particles in the bed (Quevedo et al., 2010). The medium pressure line supplied gas through a 254 μm micro-nozzle to assist in the fluidization when necessary. Pressure taps

were located above the distributor and at the exit of the column to measure pressure drop of the bed. Three mass flow meters were used to measure the flow exiting the column at ambient pressure. The flow meters had ranges from 0-1, 0-5 and 0-20 L/min.

Changes in non-dimensional pressure drop and bed expansion with gas velocity were recorded to study the hydrodynamic behavior of the bed. Non-dimensional variables were used for comparison purposes between experimental results. Non-dimensional pressure drop was obtained by dividing the actual pressure drop ΔP, by the apparent weight of the bed W/A. Similarly, the non-dimensional bed height was obtained by dividing the actual bed height H, by the initial bed height at zero flow conditions H_0.

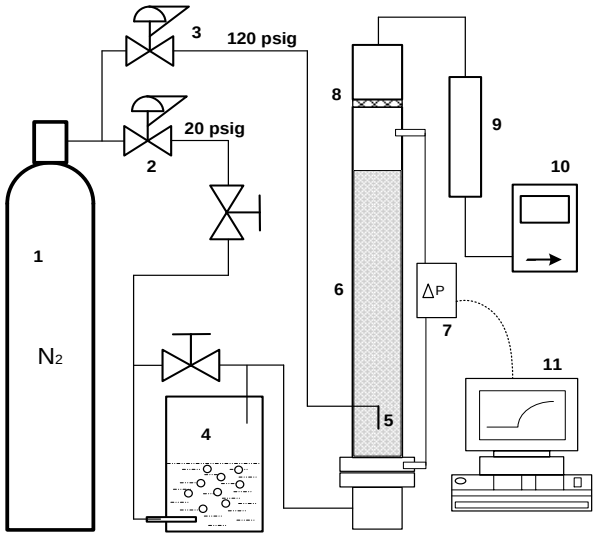

Figure 2.5. Schematic diagram of the fluidized bed setup. (1) compressed N_2 cylinder, (2) and (3) pressure regulators for low and high pressures, (4) alcohol-water solution, (5) micro-nozzle, (6) fluidization column, (7) differential pressure transmitter, (8) pre-filter, (9) HEPA filter, (10) flow meter and (11) computer (Quevedo et al., 2010).

2.3 Results and Discussion

2.3.1 TGA-DSC measurements. TGA-DSC analysis of Triameen/aerogel and Duomeen/aerogel samples under nitrogen flow was used to quantify the amine loading into the aerogels (see Figures 2.5 and 2.6). The analysis of the unmodified aerogels is shown in Figure 2.7 for comparison purposes. Three main steps of thermal decomposition were observed on the TGA curves of the modified aerogel samples. The first step takes place at 50-200 °C, and is accompanied by an endothermic peak. The mass loss in that temperature range corresponds to the evaporation of previously absorbed water. The Triameen/aerogel sample showed the highest mass loss in this temperature range. The second step, in the range 200-300 °C, corresponds to the amine decomposition. In this step the Triameen/aerogel showed a slightly higher mass loss than the Duomeen/aerogel. The third step occurs in the temperature range 300-500 °C, which corresponds to mass loss due to decomposition or oxidation of the $-CH_3$ surface groups of the aerogels. This step is also observed in the analysis for the unmodified aerogels in Figure 2.7, although in this case the decomposition continues up to 700 °C. Of the two modified samples the Duomeen/aerogel had the highest mass loss in this step.

The mass loss observed in 200-300 °C was 40% for the Triameen/aerogel sample and 35% for the Duomeen/aerogel sample, which corresponds to 1.33 and 1.38 grams of amine per grams of aerogel, respectively.

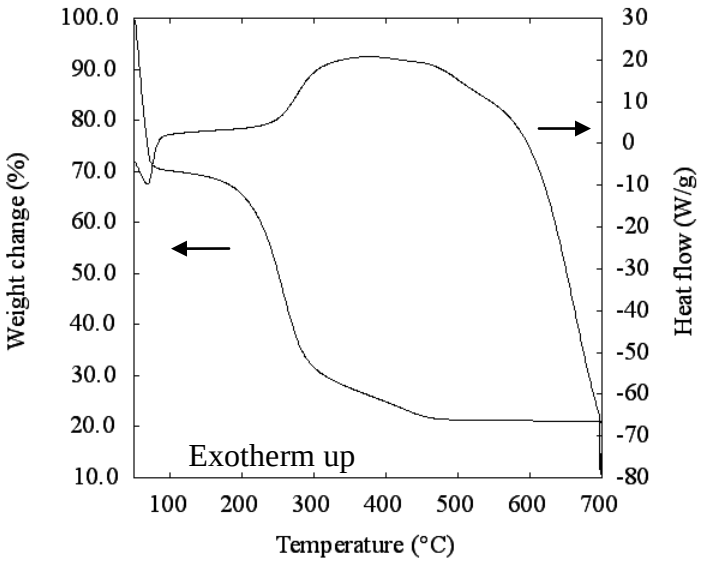

Figure 2.6. TGA/DSC of Triameen-modified aerogel under nitrogen atmosphere.

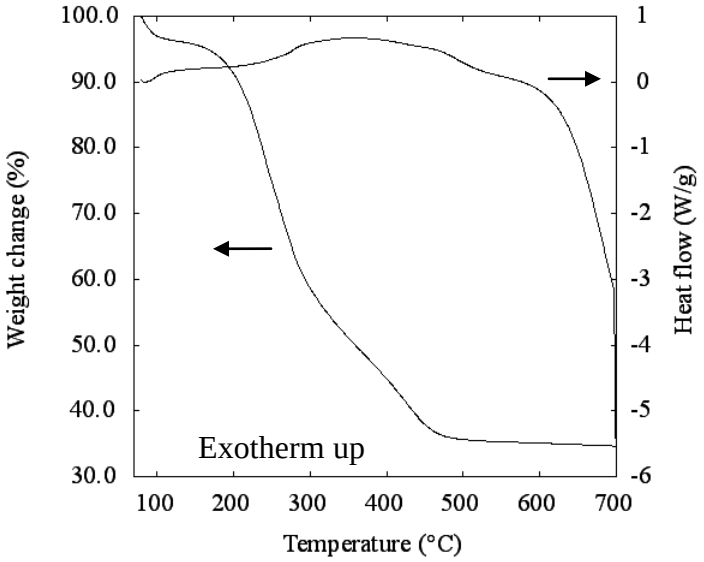

Figure 2.7. TGA/DSC of Duomeen-modified aerogel under nitrogen atmosphere.

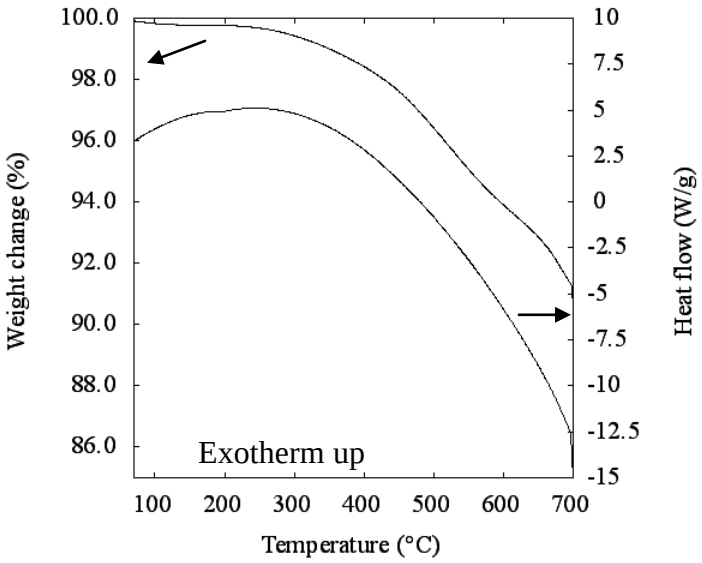

Figure 2.8. TGA/DSC of unmodified aerogel under nitrogen atmosphere.

2.3.2 CO_2 adsorption measurements in microbalance.

2.3.2.1 Physical adsorption samples. Triameen T, Duomeen T and PEI were immobilized in hydrophobic aerogels and CO_2 uptake was measured for each sample under pure CO_2. One sample prepared with Duomeen T and hydrophilic aerogels was tested with pure CO_2 to observe how the aerogel hydrophobicity affects the CO_2 uptake. In addition, one sample of Triameen modified aerogels was tested in a simulated flue gas stream with $P_{CO2} = 0.12$ and $P_{N2} = 0.88$. Table 2.2 summarizes the experimental conditions and CO_2 adsorption results obtained with each sample.

Table 2.2

CO_2 uptake and experimental conditions of sorbents prepared by physical adsorption

Surfactant	Aerogel surface	P_{CO2}	Sample wt. (g)	CO_2 uptake (mmol/g)
Triameen	Hydrophobic	1.0	0.059	1.60
Triameen	Hydrophobic	0.12	0.059	1.17
Duomeen	Hydrophobic	1.0	0.079	1.63
Duomeen	Hydrophilic	1.0	0.123	1.43
PEI	Hydrophobic	1.0	0.014	1.05

As shown in Figures 2.8-2.11 all samples adsorbed CO_2 within the first 10 minutes of the run. Duomeen/aerogel sample had almost the same CO_2 uptake as the Triameen/aerogel sample. This agrees with what was obtained by the TGA analysis, that the amine loading for the two samples was similar. The Triameen/aerogel sample tested in a simulated flue gas stream (Figure 2.8) was still able to adsorb CO_2, although adsorption decreased by 27%. Still, this is an indication that the sorbent could adsorb CO_2 at the low concentrations found in flue gases. The sample prepared with Duomeen T and hydrophobic aerogels adsorbed 14% more CO_2 per gram of sorbent than the one prepared with hydrophilic aerogels. The sample of aerogel modified with PEI had the lowest uptake of all samples. It was also lower than the uptake of other PEI modified adsorbents reported in literature (2-3 mmol/g) (Sanz et al., 2010; Xu et al., 2002). Although the amine loading for this sample was not measured using TGA, it is possible that the amount of PEI was not sufficient to coat the aerogel surface.

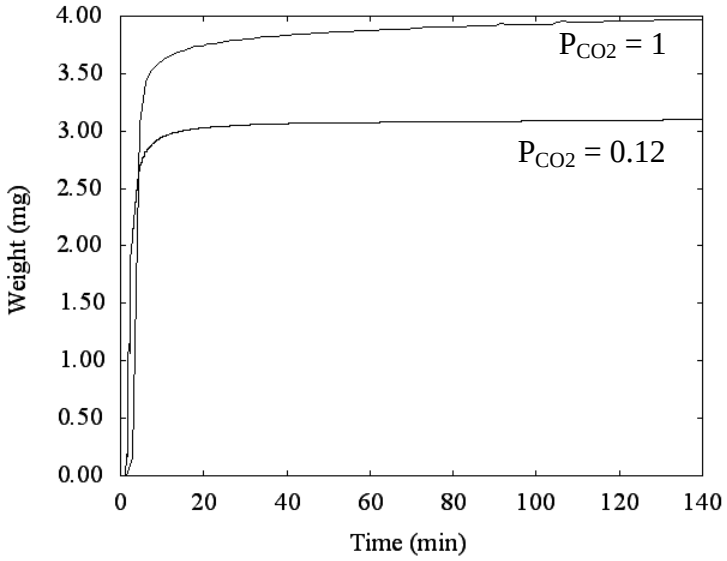

*Figure 2.9.*Weight of CO_2 adsorbed in a sample of hydrophobic aerogel modified by physical adsorption of Triameen T at P_{CO2} = 1 and P_{CO2} = 0.12 (P_{N2} = 0.88). Sample weight = 0.059 g.

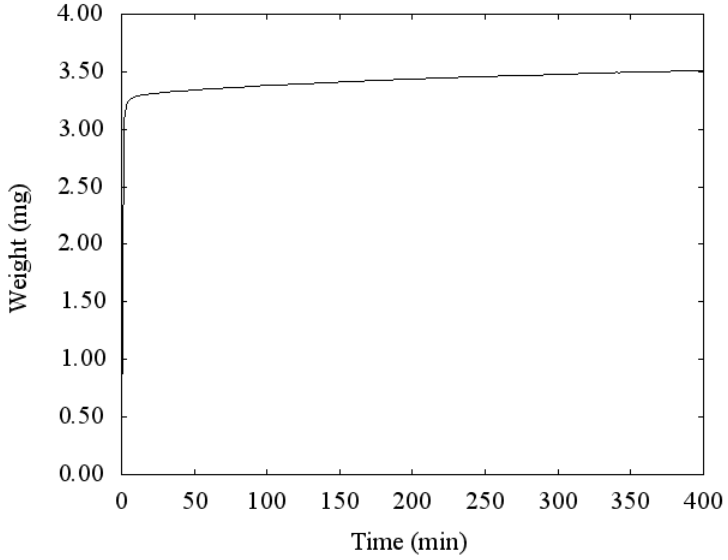

*Figure 2.10.*Weight of CO_2 adsorbed in a sample of hydrophobic aerogel modified by physical adsorption of Duomeen T. Sample weight = 0.079 g.

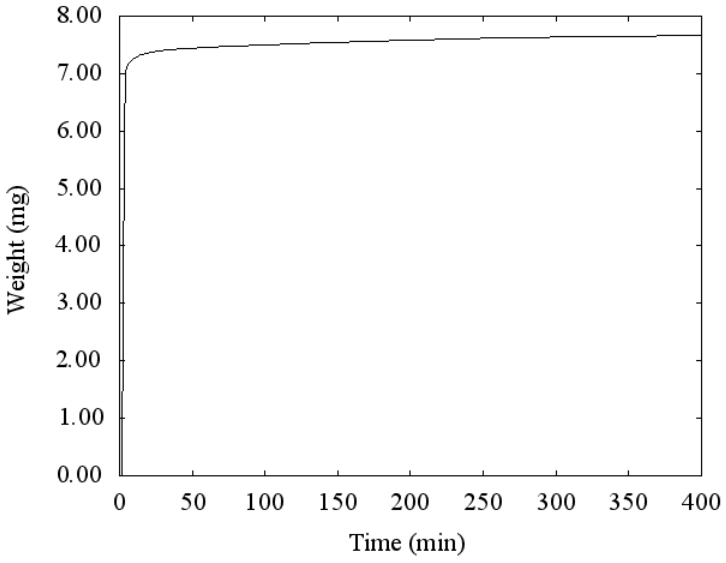

*Figure 2.11.*Weight of CO_2 adsorbed in a sample of hydrophilic aerogel modified by physical adsorption of Duomeen T. Sample weight = 0.123 g.

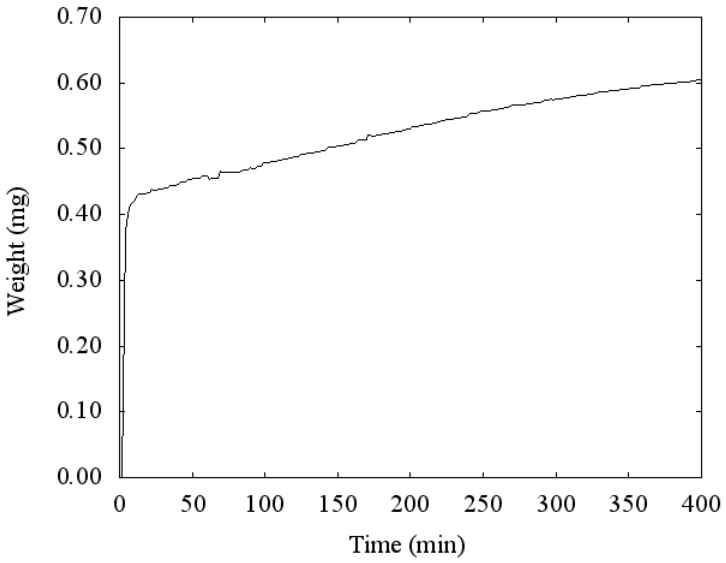

*Figure 2.12.*Weight of CO_2 adsorbed in a sample of hydrophobic aerogel modified by physical adsorption of PEI. Sample weight = 0.014 g.

2.3.2.2 MAIC samples. Four samples were prepared using hydrophobic silica aerogels and hydrophilic Aerosil 200 as substrates. Table 2.3 summarizes the experimental conditions and the CO_2 uptake of each sample.

Table 2.3

CO_2 uptake and experimental conditions of samples prepared by MAIC process

Substrate	Surfactant	Sample wt. (g)	CO_2 uptake (mmol/g)
Aerogel	Triameen	0.011	0.20
Aerogel	γ-APS	0.013	0.16
Fumed silica	Triameen	0.017	0.10
Fumed silica	γ-APS	0.010	0.00

All samples (Figures 2.12-2.15) showed a similar behavior: a quick weight loss followed by a slow weight gain. The low CO_2 adsorption took 24 hours and did not vary significantly with the different substrates and surfactants used. This adsorption behavior is similar to that of unmodified aerogels (Figure 2.18), which do not adsorb CO_2. This suggests that not enough amine was coated on the substrates. This could be a result of diluting the paste surfactant in water to obtain a liquid or gel that could be spread by MAIC.

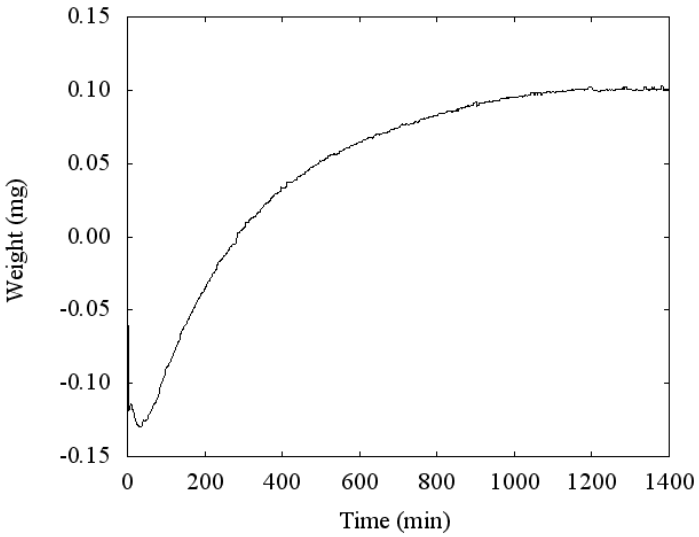

*Figure 2.13.*Weight of CO_2 adsorbed in a sample of aerogel modified by MAIC of Triameen T. Sample weight = 0.011 g.

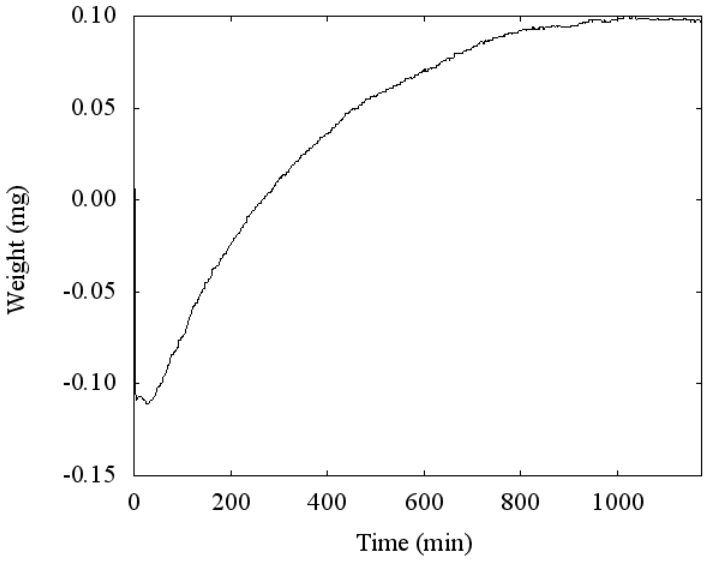

*Figure 2.14.*Weight of CO_2 adsorbed in a sample of aerogel modified by MAIC of γ-APS. Sample weight = 0.013 g.

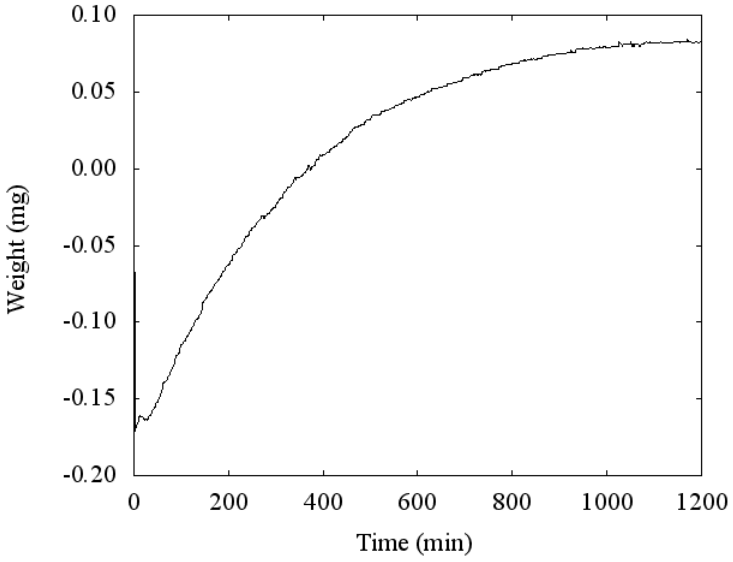

*Figure 2.15.*Weight of CO_2 adsorbed in a sample of Aerosil 200 modified by MAIC of Triameen T. Sample weight = 0.017 g.

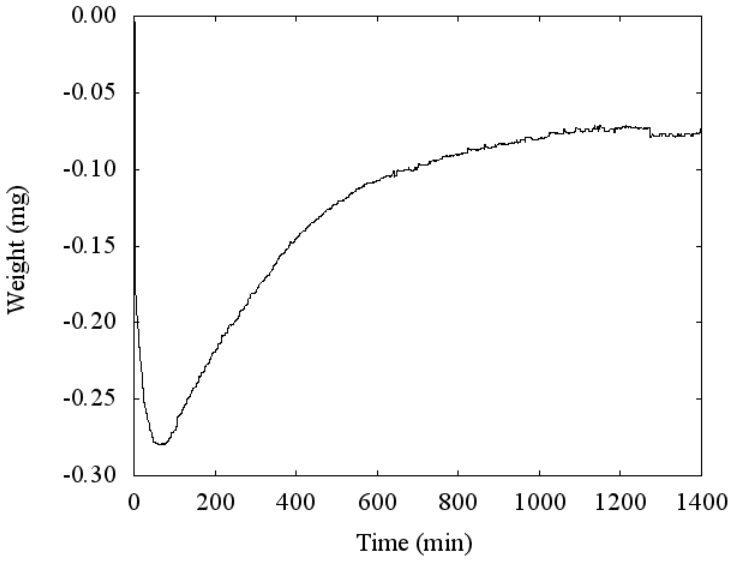

*Figure 2.16.*Weight of CO_2 adsorbed in a sample of Aerosil 200 modified by MAIC of γ-APS. Sample weight = 0.010 g.

The initial weight loss can be explained as follows. Prior to the adsorption measurements the sample is weighed under a nitrogen flow rate of 100 mL/min until the weight becomes constant (1-3 hours). Typically, a weight loss is observed during this step, which varies from sample to sample. For example, the aerogel sample modified by MAIC of Triameen T (Figure 2.16) had a weight loss of 7 mg, whereas the sample of unmodified aerogels (Figure 2.17) lost 5.3 mg. This weight loss is attributed to impurities purging out of the aerogels pores.

Once the sample is weighed, the gases are switched from nitrogen to CO_2 at the same flow rate to start the adsorption measurements. Within the first 5 minutes, a small weight loss is observed. These amounts are very small compared to the amounts lost due to the purge of impurities. The samples mentioned above had weight losses of 0.13 and 0.20 mg, respectively. Because nitrogen is not completely inert, it is possible that the small amount represents the desorption of

some nitrogen that had weakly adsorbed on the sample surface during the sample weighing step. The fast desorption is due to the weak adsorption. The following slow weight increase observed in the MAIC samples is due to the chemical adsorption of CO_2 and the formation of carbamates. This is not seen in the samples prepared by physical adsorption method probably because the pores of those samples are filled with the amine/water mixture, so there is no place for the nitrogen to get adsorbed.

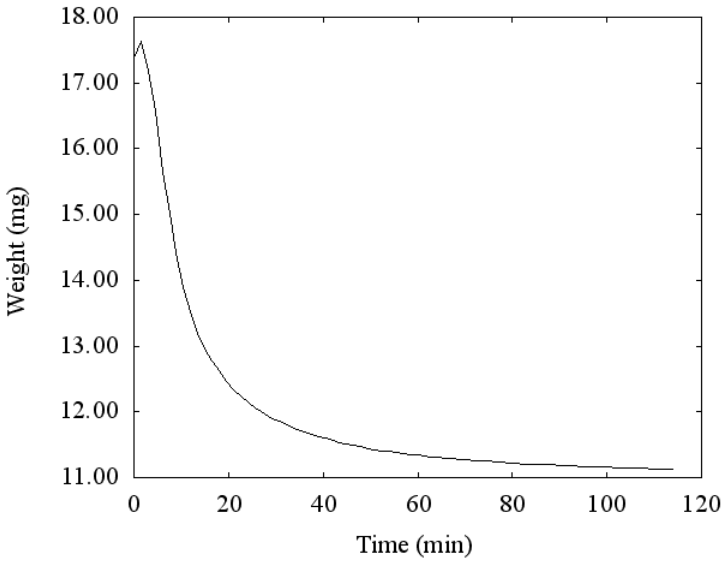

Figure 2.17. Weight of aerogel sample modified by MAIC of Triameen T (0.011 g).

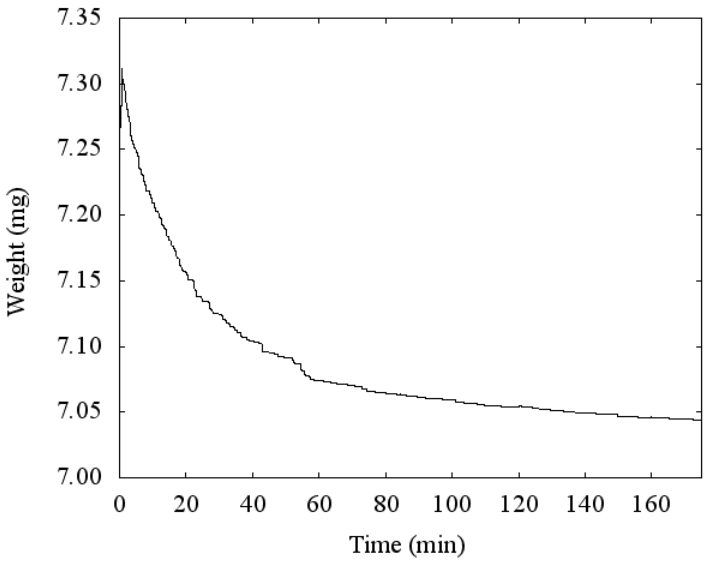

Figure 2.18. Sample weight of unmodified hydrophobic aerogels (0.00705 g).

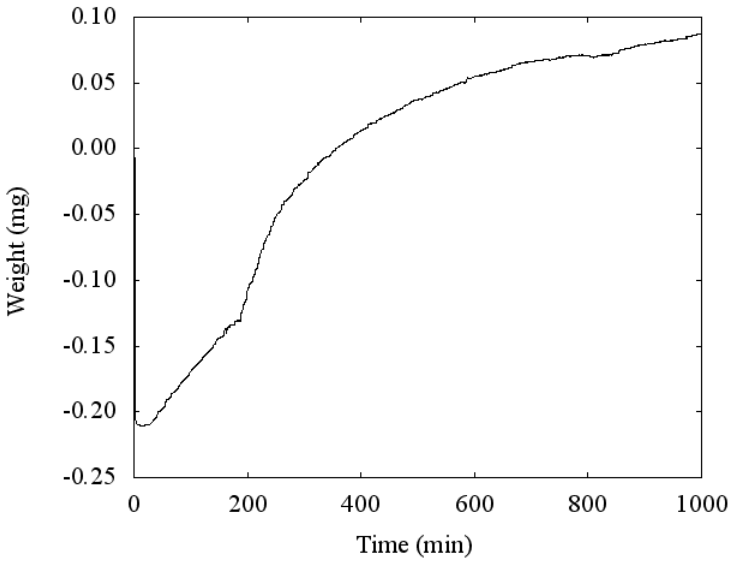

Figure 2.19. Weight of CO_2 adsorbed in a sample of unmodified aerogels (0.0001 g).

2.3.2.3 ALD samples. Table 2.4 summarizes the experimental conditions used to prepare the samples, and the CO_2 uptake of each of them. Figures 2.19-2.25 show the CO_2 weight gain by each sample.

Like with the MAIC samples, the CO_2 adsorption obtained with ALD samples 1-6 was very low and slow, indicating that there was not enough amine coating on the surface. It is possible that amine precursors could not react with the entire surface of the aerogel because the trimethylsilyl terminal groups on the surface are very stable at the synthesis conditions used to prepare the samples, e.g. temperatures, pressures, cycle time. Because in highly porous substrates the transport of precursors in and out of the pores much slower than in planar surfaces, larger doses of precursors and longer exposure and purge times play an important role in coating the ALD layer (Ritala et al., 2002). The initial weight loss observed in samples 1-6 is due to the same phenomenon explained above for the MAIC samples.

Table 2.4

CO_2 uptake and experimental conditions of samples prepared by ALD process

ID	Pre-cursors	Temps. (°C)	Sample wt. (g)	CO_2 uptake (mmol /g)	Description
1	NH_3	350-500	0.020	0.14	Raised temp. while dosing NH_3, no ALD
2	BN, NH_3	23-500, 350	0.018	0.52	Increased temp. from 23-500°C, decreased to 350°C, 1 cycle of BN ALD
3	NH_3	23-500	0.023	0.23	Raised temp. while dosing NH_3, no ALD
4	NH_3	25-300	0.011	0.12	Increased temp. from 25-300°C, held one hour at 300°C, 100 torr
5	TDMAS, NH_3	500	0.025	0.17	1 cycle Si_3N_4 ALD
6	ETA	175	0.024	0.19	No ALD
7	NH_3	500	0.022	1.23	Raised temp. while dosing NH_3, no ALD

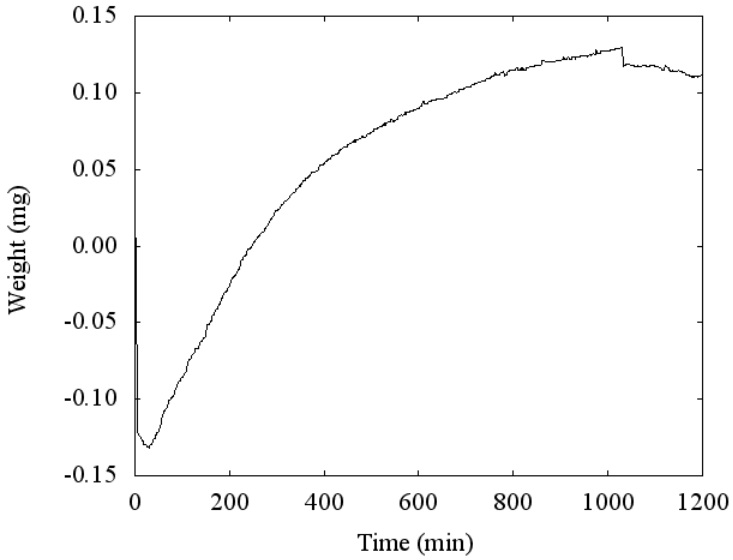

*Figure 2.20.*Weight of CO_2 adsorbed in a sample of aerogel modified by ALD (sample 1). Sample weight = 0.020 g.

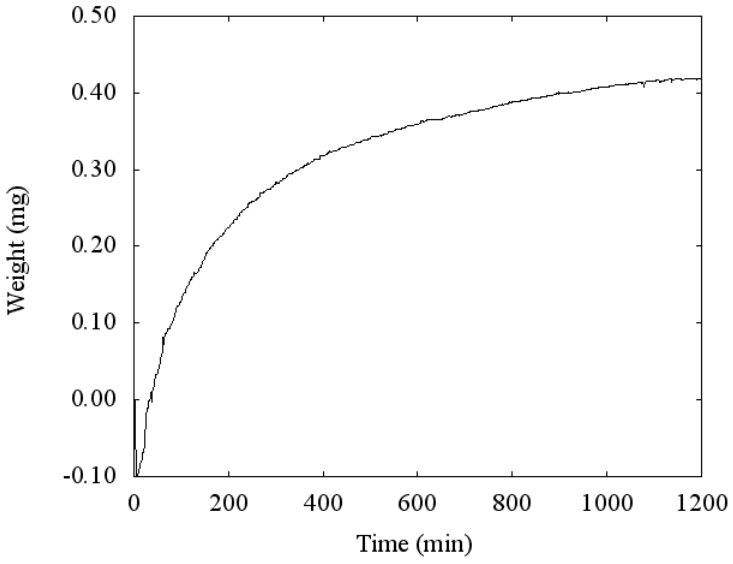

*Figure 2.21.*Weight of CO_2 adsorbed in a sample of aerogel modified by ALD (sample 2). Sample weight = 0.018 g.

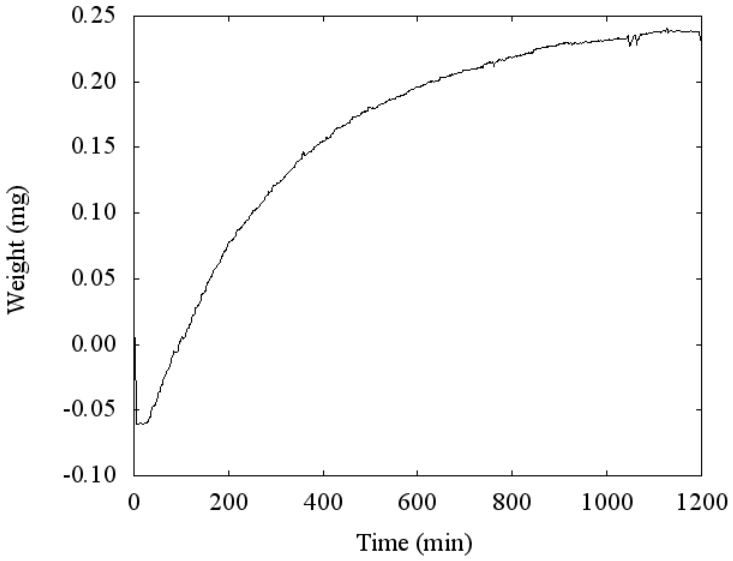

*Figure 2.22.*Weight of CO_2 adsorbed in a sample of aerogel modified by ALD (sample 3). Sample weight = 0.023 g.

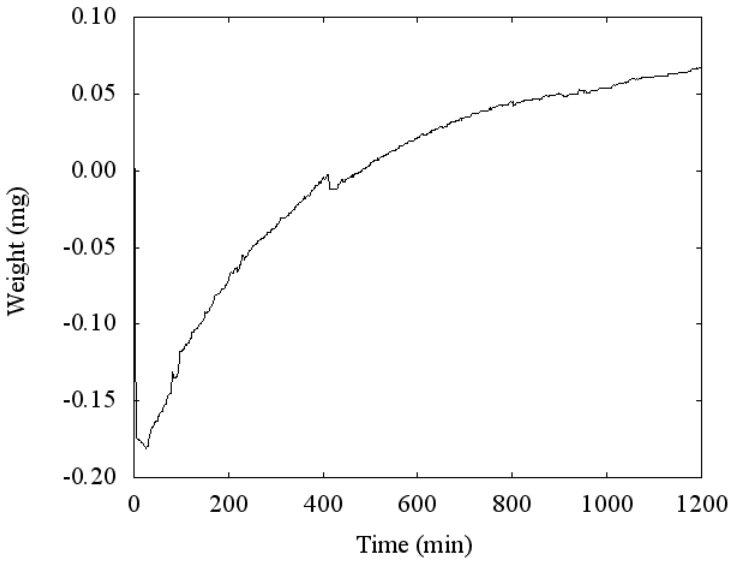

*Figure 2.23.*Weight of CO_2 adsorbed in a sample of aerogel modified by ALD (sample 4). Sample weight = 0.011 g.

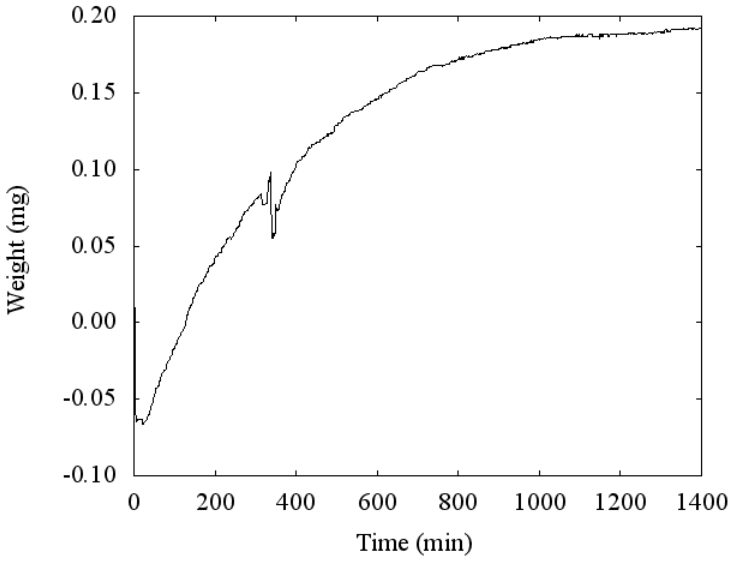

*Figure 2.24.*Weight of CO_2 adsorbed in a sample of aerogel modified by ALD (sample 5). Sample weight = 0.025 g.

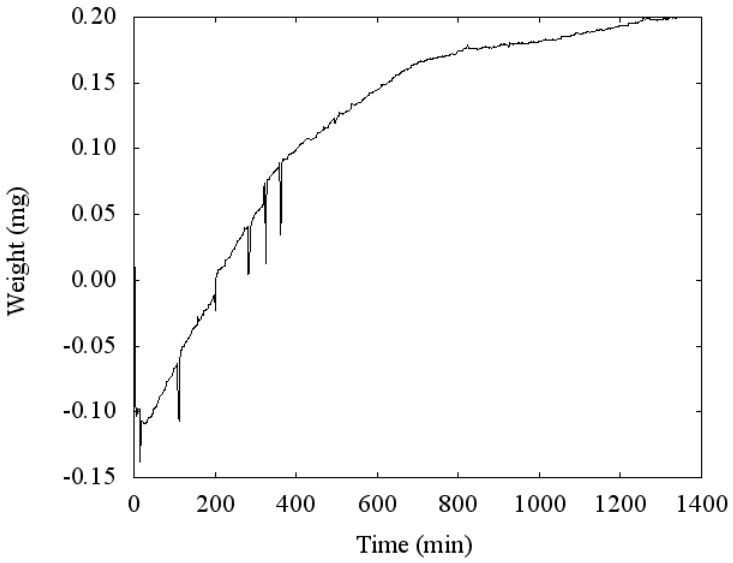

Figure 2.25. Weight of CO_2 adsorbed in a sample of aerogel modified by ALD (sample 6). Sample weight = 0.024 g.

Hydrophilic aerogels (prepared by oxidizing them in the oven at 400 °C overnight) were amine-coated by using ALD at atmospheric pressures. CO_2 adsorption capacity of this sample in dry conditions was 1.23 mmol/g, the highest adsorption of all the ALD samples. Changing from vacuum to atmospheric pressures allowed the precursors to be dosed at higher flow rates. As discussed by Ritala et al. (2005), higher flow rates may facilitate the transport of the precursors through the pores of the substrate, allowing more surface area to be coated by the amines. Using hydrophilic aerogels, by removing the trimethylsilyl terminal groups upon heating, may have also helped in improving the amine layer deposition. This uptake is comparable to the uptake of the samples modified by physical adsorption of Triameen T and Duomeen T. However, the adsorption of this sample was slower as shown by the curve in Figure 2.25.

Table 2.5

Uptake of hydrophilic aerogels prepared by ALD at atmospheric pressure

Sample	Gas	Dry/Humid	Uptake mmol/g
hydrophilic aerogel + amines	CO_2	dry	1.23
hydrophilic aerogel + amines	CO_2	humid	3.20
hydrophilic aerogel	N_2	humid	51.21 (vapor)

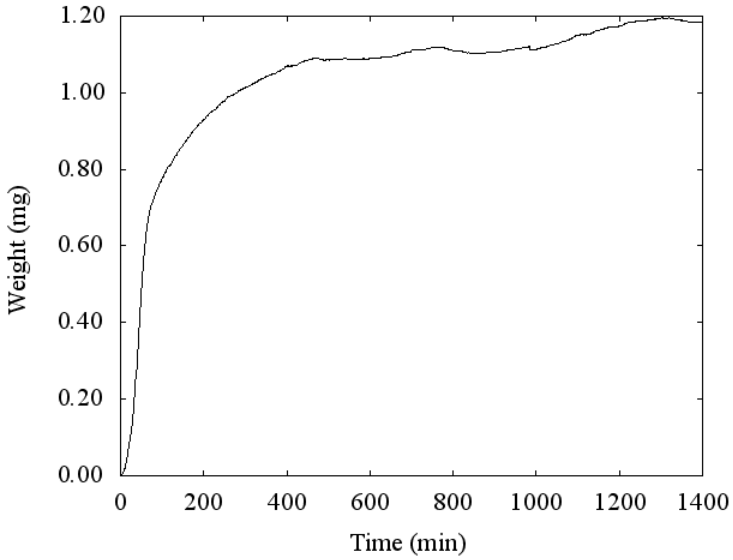

Figure 2.26. Weight of CO_2 adsorbed in a sample of aerogel modified by ALD under dry CO_2 (sample 7). Sample weight = 0.022 g.

The adsorption capacity of this sample was also tested with a gas stream containing CO_2 and water vapor. Studies have shown that the presence of water enhances CO_2 adsorption on amine-modified sorbents (Huang et al., 2003; Hiyoshi et al., 2005). The mechanisms for CO_2 removal using amines (pathways 1 and 2 in Chapter 1) show that the water promotes the bicarbonate reaction which requires only 1 mol of amine for each mol of CO_2, whereas the absence of water promotes carbamate formation which requires 2 mol of amine for each mol of CO_2.

When exposed to humid gas the calculated uptake, assuming that CO_2 was the only gas adsorbed, was 25.40 mmol/g, which is extremely high in comparison to the dry CO_2 uptake (Table 2.5). This suggests that the sample adsorbed water vapor in addition to CO_2. The calculated uptake assuming that the sample adsorbed only water vapor was 59.03 mmol/g. To know how much water vapor is

adsorbed by the amine-modified sample, a sample of hydrophilic aerogels with no amine coating was run under humid N_2. The uptake curves (Figures 2.26 and 2.27) show the same slow increase in weight until saturation is reached. The water vapor uptake of the hydrophilic aerogel sample was 51.21 mmol/g, which confirms that the sample adsorbs large amounts of water vapor due to its hydrophilic nature. The CO_2 uptake of the amine-modified sample was estimated assuming that it was equivalent to the difference of the water vapor uptakes between the amine-modified sample and the hydrophilic aerogel sample with no amines. The estimated CO_2 uptake was 3.20 mmol/g, which is 1.6 times higher than the CO_2 uptake under dry gas. This increase in the CO_2 uptake may have been due to the effect of water vapor on the CO_2-amine reaction. However more experiments need to be performed to confirm this explanation.

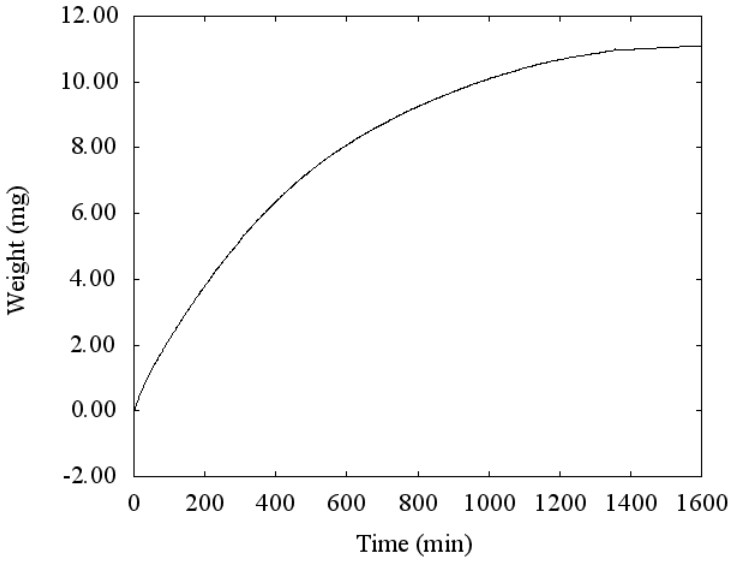

Figure 2.27. Weight of CO_2 and water vapor adsorbed in a sample of aerogel modified by ALD under humid CO_2 (sample 7). Sample weight = 0.010 g.

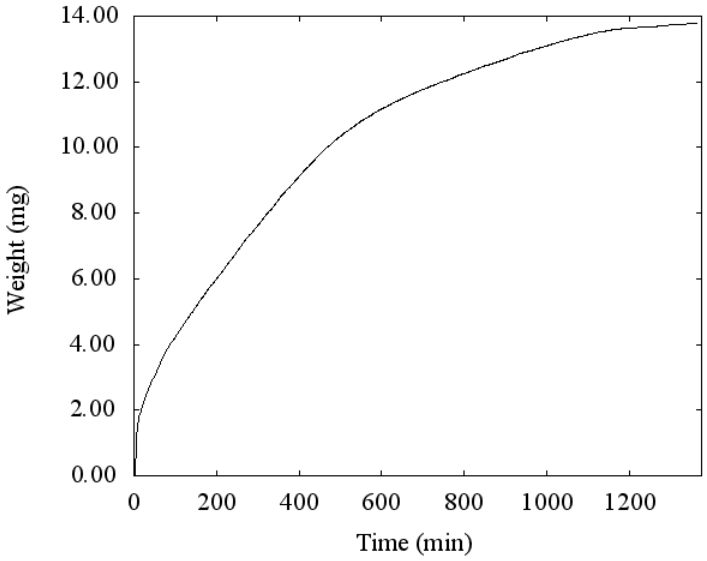

Figure 2.28. Weight of H_2O adsorbed in a sample of hydrophilic aerogels. Sample weight = 0.014 g.

2.3.3 Fluidization of aerogels. Hydrophobic and hydrophilic unmodified aerogels were fluidized in a 1 inch column with nitrogen fluidizing gas at superficial velocities of up to 3.5 cm/s. Figures 2.28 and 2.29 show the non-dimensional pressure drop and the bed expansion as a function of gas velocity for a bed of hydrophobic aerogels. The non-dimensional pressure drop in Figure 2.28 plateaus at one, indicating that complete fluidization of the bed was achieved. The aerogels exhibited an APF type behavior with a minimum fluidization velocity, u_{mf}, of 0.06 cm/s (shown by the red vertical lines), and a bed expansion of 3 times the original height.

On the other hand, hydrophilic aerogels showed an ABF type behavior with vigorous bubbling. Figures 2.30 and 2.31 show the non-dimensional pressure drop and bed expansion plotted against gas velocity for hydrophilic aerogels. The u_{mf} doubled compared to that of the hydrophobic aerogels, and the non-

dimensional pressure drop was much less than 1, indicating that complete fluidization was not achieved, i.e. not all of the aerogel particles participated in the fluidization. There are three explanations for this behavior: (1) the water adsorbed by the hydrophilic aerogels causes liquid bridges to exist between the aerogel particles and these result in strong, interparticle forces even after the water is evaporated during the drying step, (2) during the oxidation of the aerogels in the oven, aerogel granules probably agglomerate into larger particles, and (3) electrostatic charge effects between the particles and the column wall may be much more prevalent for the hydrophilic particles than for the hydrophobic ones.

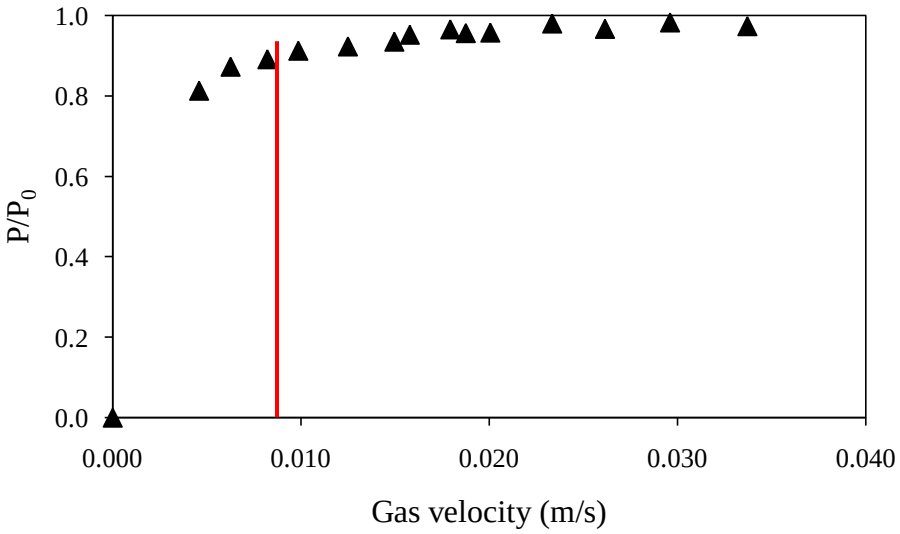

Figure 2.29. Non-dimensional pressure drop of hydrophobic aerogels as function of gas velocity. Sample weight = 4.504 g.

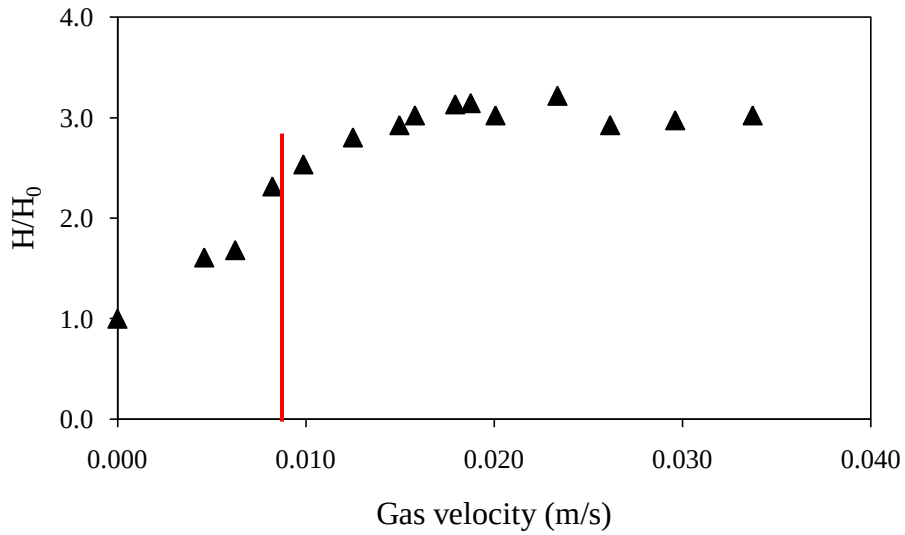

Figure 2.30. Non-dimensional bed expansion of hydrophobic aerogels as function of gas velocity. Sample weight = 4.504 g.

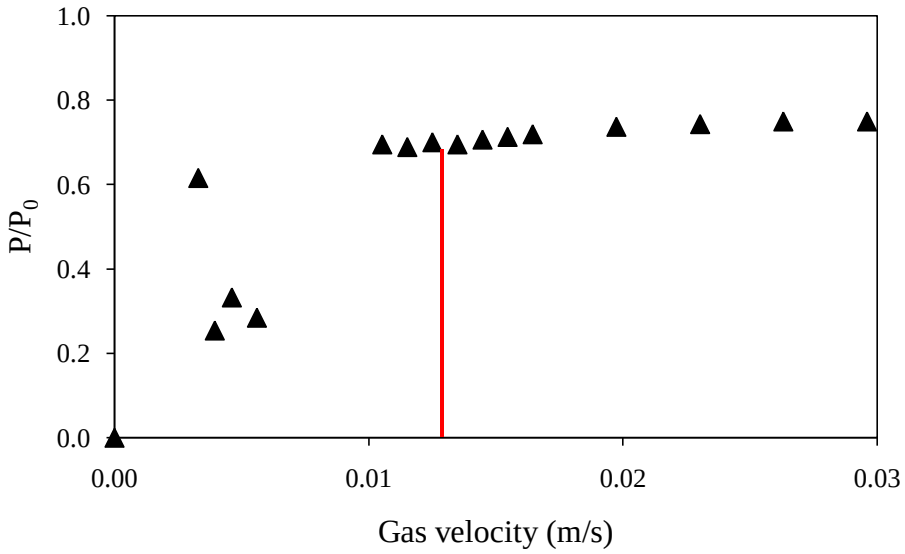

Figure 2.31. Non-dimensional pressure drop of hydrophilic aerogels as function of gas velocity. Sample weight = 2.140 g.

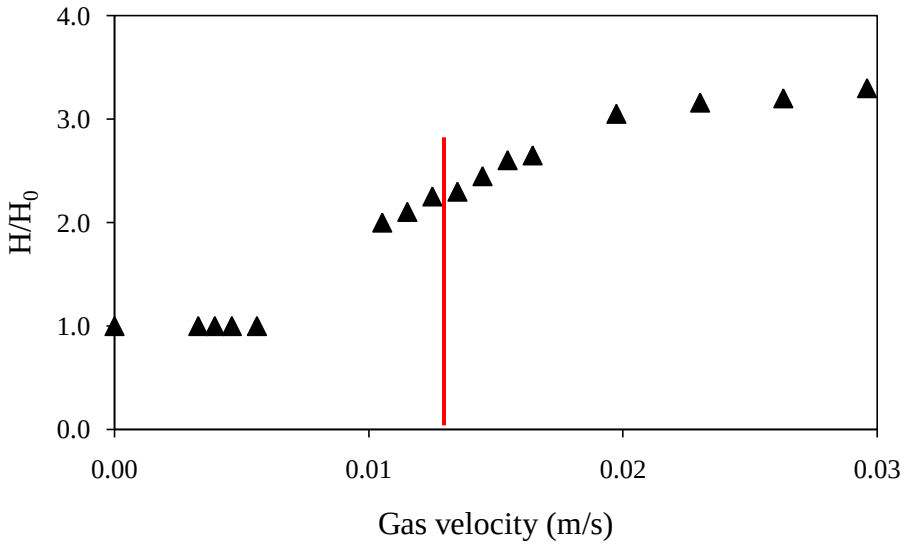

Figure 2.32. Non-dimensional bed expansion of hydrophilic aerogels as function of gas velocity. Sample weight = 2.140 g.

Duomeen modified aerogels were fluidized in a 3 in acrylic column equipped with a micro-nozzle with a diameter of 254 µm. About 86 grams of the powder, sieved to under 500 µm, were loaded into the column. Initially, N_2 gas was bubbled through ethanol for 20 minutes before entering the column to reduce electrostatic charge effects. Then, the powder was processed with dry N_2 flowing through the distributor at a superficial gas velocity of 5.4 cm/s for 15 minutes. Then, the micro-jet assistance was started and the powder was processed for 60 minutes at a total superficial velocity of 6.1 cm/s. The heavy powder exhibited ABF type behavior with incomplete fluidization and no significant bed expansion while the gas was flowing through channels in the bed. The bed was vigorously bubbling and was very unstable. The powder on the surface of the bed was suspended by the gas and was sticking to the wall of the column. As it happened with hydrophilic aerogels, liquid bridges may have formed between the particles

when they were wet during preparation. These may have turned into solid bridges upon drying, forming agglomerates. At the operating conditions used in this experiment, the combined action of the gas flowing through the distributor at low velocity and the high velocity of the micro-jet is unable to break the agglomerates. Increasing the superficial gas velocity through the distributor, and/or using a nozzle with smaller diameter to increase the radial velocity gradient at the exit of the nozzle, and therefore the micro-shear acting on the agglomerates, could improve the fluidization of the powder.

2.4 Conclusions

Based on the experimental results presented above, it can be concluded that the amine functionalization of aerogels by physical adsorption resulted in the highest CO_2 adsorption capacities of all the synthesis methods explored in this study. Although the amine coated surfaces were not analyzed, the CO_2 adsorption results suggest that the hydrophobic aerogels samples prepared by MAIC and ALD did not have sufficient amine coating. In the case of the MAIC samples, surfactants with lower viscosities should be used at higher concentrations to obtain a uniform amine coating. In the case of ALD samples, doing ALD using ammonia as a precursor as a half step at atmospheric pressures appears to be the right direction to improve amine coating. The use of atmospheric pressures allows the precursors to be in contact with the entire surface area of the aerogels. Hydrophilic aerogels may provide a better surface for amine functionalization than hydrophobic aerogels at the conditions studied, but water vapor cannot be added since it is readily adsorbed by the hydrophilic aerogels. The CO_2 adsorption

capacities of the most successful sorbents are still lower than the amount necessary to compete with current CO_2 separation processes.

Hydrophobic aerogels have fluidization behavior of APF type characterized by a smooth fluidization without bubbles, and a fluidized bed expansion of several times the initial height. Hydrophilic aerogels show an ABF behavior with vigorous bubbling and incomplete fluidization. This behavior is due to strong interparticle forces that may form large agglomerates. Another explanation could be that the electrostatic charge effects between the particles and the column wall are larger for hydrophilic aerogels than for hydrophobic ones.

Duomeen T modified aerogels prepared by a physical adsorption method show a fluidization behavior of ABF type. Large bubbles rising up through the bed, and elutriation of particles on the top of the bed were observed even when the microjet was used to assist the fluidization. Like with hydrophilic aerogels, this could be due to strong interparticle forces formed during preparation that led to large agglomerates that are difficult to fluidize. To overcome these problems, some operating conditions such as the superficial gas velocity through the distributor, upstream pressure to the micro-nozzle, and nozzle size may need to be optimized.

Chapter 3

METAL-ORGANIC FRAMEWORK-5 MEMBRANES

3.1 Introduction

In Chapter 2, the synthesis of amine functionalized aerogels, and their CO_2 adsorption capacity are described. This chapter presents another approach to separate and capture CO_2: membrane separation. The chapter focuses on the synthesis and characterization of MOF-5 membranes via in situ and secondary growth methods. Permeance and selectivity of single gases are measured for each membrane. Comparison of characteristics and performance of the membranes is discussed.

3.2 Experimental

3.2.1 Synthesis of MOF-5 membranes. MOF-5 membranes were synthesized by two methods: secondary growth and in situ hydrothermal methods. The membranes were synthesized on homemade alumina (α-Al_2O_3) support disks of 20 mm in diameter and 2 mm thick made with alumina powder (Alcoa, A-16). The normal pore size was around 200 nm and the porosity was about 45%. The supports were prepared by mixing 2.1 grams of alumina powder with 10% de-ionized water used as a binder. The mixture was slowly pressed in a stainless steel mold at 20,000 lb_f (Carver) for 5 minutes. The supports were kept for two days in a controlled humidity oven at 40 °C and 60% relative humidity. Then, the supports were sintered for four days using a temperature program at 600-1260 °C (see Appendix A for details). This was followed by the preparation of the surface of the supports for membrane growth. The surfaces were polished using SiC paper

(#500, #800, #1200) on a Metaserve 2000 polisher, and ultrasonic bath was used to remove residual debris. Finally, the supports were stored in the controlled humidity oven at the same conditions until they were used.

The secondary growth synthesis method consisted of three main steps: synthesis of MOF-5 crystals (seeds) and the preparation of their suspension, dip coating of alumina supports to grow MOF-5 seeds layer, and secondary growth. MOF-5 seeds were synthesized by using a method similar to the one reported by Panella et al. (2006). This method has been optimized for the fast synthesis of MOF-5 crystals. The solution was prepared by dissolving 1.664 g of zinc nitrate and 0.352 g of BDC in 40 mL of previously degassed DMF solvent. The solution was transferred to a glass vial and sealed. The vial was heated at 130 °C in an oil bath for 4 hours under autogenous pressure. After 4 hours, the vial was removed from the oil bath and cooled down to room temperature. The MOF-5 crystals were filtered and washed with DMF to remove any unreacted material. Then, the crystals were immersed in 50 mL of chloroform at 70 °C for 3 days. The chloroform was replenished daily. Finally, the crystals were dried at 90 °C under vacuum overnight. Prior to preparing the suspension, the crystals were ground in a ball mill grinder to obtain uniform particle size. The suspension (2 wt% MOF-5) was prepared by vigorous stirring for 1-3 hours, followed by sonication for another 1-3 hours. To coat the seed layer on the surface of the alumina support, a dry, polished support was dip coated into the suspension for 5 seconds and dried at 50 °C overnight. This step was repeated up to three times to obtain a thicker layer.

The secondary growth step was performed to grow the seed layer into a continuous membrane. The secondary growth solution consisted of 0.832 g of zinc nitrate and 0.176 g of BDC dissolved in 40 mL of degassed DMF. Next, 0.137 g of N-ethyldiisopropylamine (EDIPA, +99.5% Acros) was slowly added under vigorous stirring. EDIPA base is used to prevent BDC from dissolving the crystals. The seeded support was held vertically by a Teflon holder, and added to the solution. The solution was sealed in a glass vial and heated to 130 °C in an oil bath for 4 hours. Once the reaction was completed, the vial was cooled to room temperature. The membrane was removed and washed three times with DMF. Then, the membrane was immersed in chloroform at 70 °C for 2 days, with daily solvent replenishment. Finally, the membrane was dried overnight at 90 °C under vacuum.

The in situ synthesis method presented in the work of Liu et al. (2009) was used in this work, with a few modifications, to synthesize MOF-5 membranes. The synthesis procedure involved dissolving 0.063 g of 1,4-benzenedicarboxylic acid (BDC, +99.9% Aldrich) in 10 mL of N, N-dimethylformamide (DMF, 99% Mallinckrodt), and loading the solution in a Teflon lined stainless steel autoclave. Then, a dry alumina support was dipped into the solution with the smooth surface facing upwards for 30 minutes. Next, 0.34 g of dehydrated zinc nitrate hexahydrate ($Zn(NO_3)_2 \cdot 6H_2O$, 99.5% Fluka) was added to the autoclave. The zinc nitrate was previously dehydrated at 80 °C under vacuum for 12 hours. The mixture was sealed and heated to 105 °C for 24 hours. Upon completion of the synthesis, the autoclave was cooled to room temperature. The membrane was

removed from the autoclave and washed three times with DMF, and then immersed in DMF for 12 hours. Solvent exchanged was done by washing the membrane three times with chloroform, followed by dipping it in 30 mL of chloroform for another 12 hours. Finally, the solvent was decanted and the membrane was dried at 60 °C for 24 hours under vacuum.

3.2.2 Membrane characterization. Characterization of MOF-5 crystals and membranes was done by scanning electron microscopy (SEM), porosimetry, X-ray diffraction (XRD), and steady state permeation of single gases. The surface morphology and membrane thickness were analyzed with a Philips FEI XL-30 scanning electron microscope operating at 20 kV. Prior to SEM observation the samples were sputtered with gold to increase their conductivity. The pore structural properties were measured by Micromeritics ASAP 2020 porosimeter with liquid nitrogen at 77 K. The N_2 adsorption and desorption isotherms were used to calculate Langmuir surface area, Brunauer-Emmet-Teller (BET) surface area, and pore volume. To determine the crystal structure, XRD diffraction data of both MOF-5 crystals and membranes were obtained from a Siemens D5000, Panalytical X'Pert Pro Diffractometer with Cu Kα radiation ($\lambda = 1.544$ Å).

Steady-state permeation of single gases was measured to study the transport through the MOF-5 pore structure. Figure 3.1 shows a diagram of the apparatus. Supported membranes were placed in a Wicke-Kallenbach type cell with the top layer facing upstream sealed with Viton O-rings. Helium and nitrogen flow was passed through the membrane and, after steady state was reached, the pressures on the feed and permeate sides were measured by pressure

meters. In addition, the flow rate was measured with a bubble flow meter. Data was taken at different pressures that were changed by a needle valve.

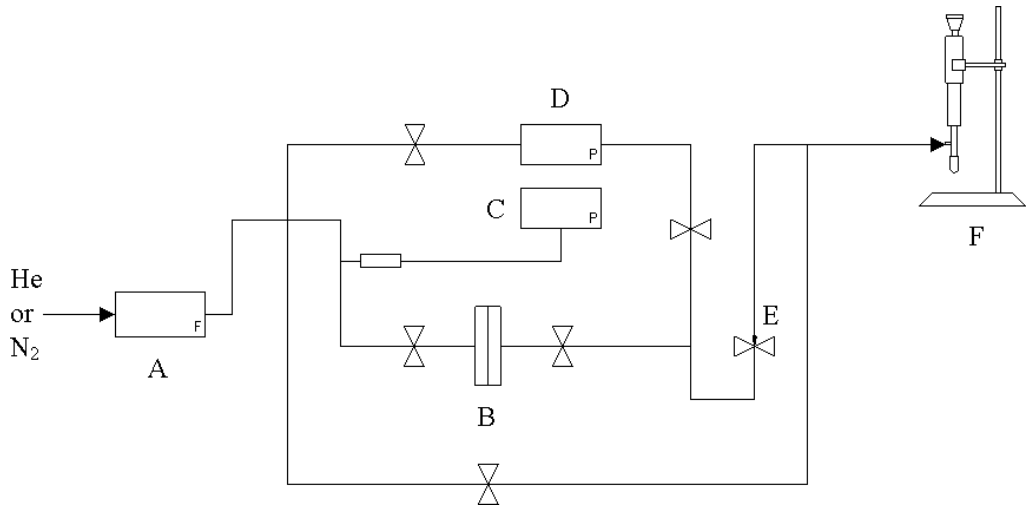

Figure 3.1. Gas permeation apparatus used for steady-state single gas permeation measurements through MOF-5 membranes. (A) mass flow controller, (B) membrane cell, (C) and (D) pressure readers, (E) needle valve, and (F) bubble flow meter.

The permeance of each gas was calculated using Equation 4 where F is the permeance ($mol \cdot m^{-2} \cdot s^{-1} \cdot Pa^{-1}$), Q is the molar flow rate ($mol \cdot s^{-1}$), S is the membrane area (m^2), and P_f and P_p are the feed and permeate pressure respectively (Pa).

$$F = \frac{Q}{S(P_f - P_p)} \tag{4}$$

$$P_{av} = \frac{(P_f + P_p)}{2} \tag{5}$$

$$F = \alpha_{av} + \beta_{av} P_{av} \tag{6}$$

Then, the permeance data was plotted as function of average pressure P_{av} (Equation 5), and regressed using Equation 6. The coefficients α_{av} and β_{av}

represent contributions to the gas transport by Knudsen and viscous flow respectively, and β_{av}/α_{av} is an estimate of the average pore size of the membrane. The coefficients were calculated by the following equations:

$$\alpha_{av} = 1.06\left(\frac{\varepsilon}{L\tau}\right)\frac{r}{\sqrt{RTM}} \tag{7}$$

$$\beta_{av} = 0.125\left(\frac{\varepsilon}{L\tau}\right)\frac{r^2}{\mu RT} \tag{8}$$

where L is the thickness of the membrane, ε is the porosity factor, τ is the tortuosity factor, r is the average pore size of the composite membrane, T is the temperature, M is the molecular weight of the gas and μ is the viscosity of the gas.

Permeance through the porous support and through the composite membranes was measured and used to calculate the permeance of the membrane layer by a subtraction method (Jayaraman and Lin, 1995). Figure 3.2 illustrates the gas permeance through a composite membrane. The different layers in the composite membrane were thought of as various resistances in series for the constant gas flow. The only unknown variable was the pressure between both layers P_m, which was calculated by solving Equation 9 for each data point taken during the experiment. The coefficients α_S and β_S were obtained from the regression analysis of the permeance through the support layer. After P_m was calculated for each data point, the permeance of the membrane layer F_{ml}, and the average pressure P_{av}, was calculated with Equations 10 and 11. Finally, F_{ml} was plotted as function of P_{av}, and the coefficients α_{ml} and β_{ml} were obtained from a regression analysis.

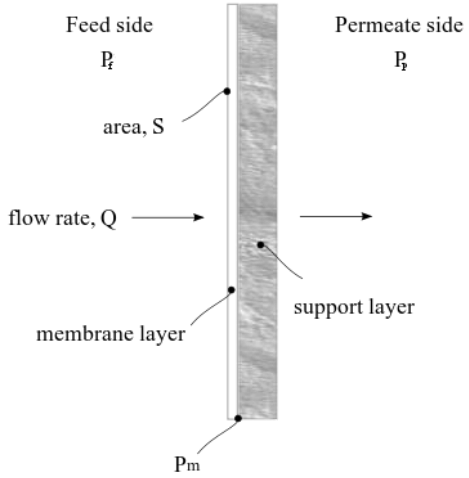

Figure 3.2. Schematic of gas permeance through a composite membrane. P_f and P_p are the pressures at the feed and permeate sides, respectively. P_m is the pressure between the membrane layer and the porous support.

$$Q = \left[\alpha_S + \beta_S\left(\frac{P_m + P_p}{2}\right)\right] \cdot S(P_m - P_p) \tag{9}$$

$$F_{ml} = \frac{Q}{S(P_f - P_m)} \tag{10}$$

$$P_{av} = \frac{(P_f + P_m)}{2} \tag{11}$$

where F_S, α_S and β_S are the permeance and coefficients obtained for the support layer, and F_{ml} is the calculated permeance through the membrane layer.

3.3 Results and Discussion

3.3.1 MOF-5 microstructure. MOF-5 crystals were synthesized to grow a seed layer in the secondary growth synthesis method. Electron microscope images of MOF-5 crystals (Figure 3.3) show well-shaped cubic single and polycrystals ranging from 40 to 100 μm in size. The nitrogen adsorption isotherm shown in Figure 3.4 is of microporous type I behavior, with an initial sharp

increase followed by a plateau at higher pressures. The BET surface area, Langmuir surface area, and average pore volume calculated for this sample are 835 m^2/g, 914 m^2/g, and 0.34 cm^3/g, respectively, and the desorption average pore width is 16.2 Å. The surface areas are in the low end of the wide range that has been reported (700-3400 m^2/g) in literature for MOF-5 synthesis by different conditions and procedures. However, the values agree with those reported by Huang et al., 2003; Tsao, et al., 2007 and Hafizovic et al., 2007. As explained by Tsao et al. (2007) and Hafizovic et al. (2007), the low surface areas can be a result of a reduction of the available pore volume due to pore-filling effects. These pore effects are attributed to the presence of $Zn(OH)_2$ species which occupy the cavities of the MOF-5 framework, and to double interpenetrated MOF-5 framework (Hafizovic et al., 2007).

The positions of the main peaks shown in the powder x-ray diffraction pattern (PXRD) presented in Figure 3.5 match well with the MOF-5 patterns reported in literature, including the groups mentioned above. The peaks are indexed by assuming that the crystals have cubic structure (Fm-3m). The unit cell parameter, a, was calculated to be 25.7 Å, which matches well with what has been reported for MOF-5 (Li et al, 1999). The variation in the intensity of the first two peaks can be attributed to the pore-filling effects discussed above, or to crystal orientation.

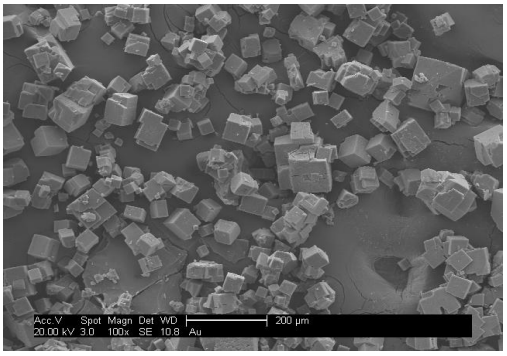

Figure 3.3. SEM image of the MOF-5 crystals prepared by hydrothermal synthesis.

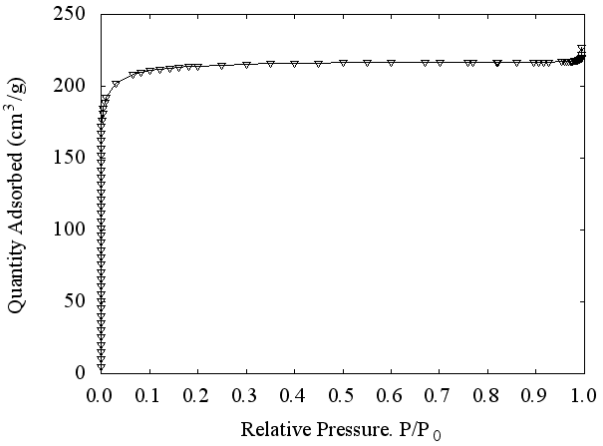

Figure 3.4. Nitrogen adsorption isotherm of MOF-5 crystals at 77 K.

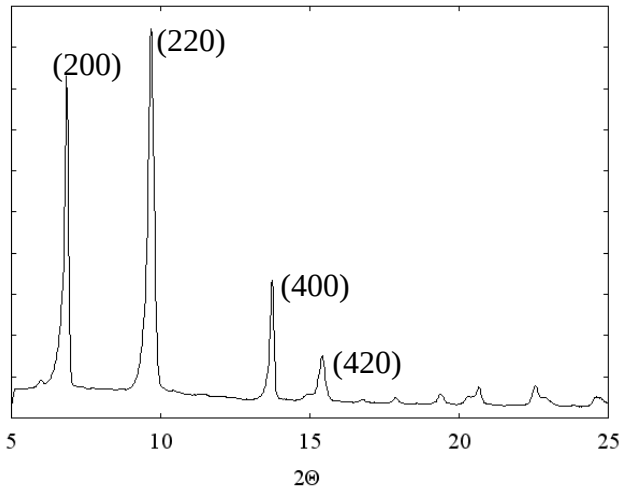

Figure 3.5. PXRD pattern of MOF-5 crystals prepared by hydrothermal synthesis.

3.3.2 XRD and SEM of MOF-5 membranes. The SEM images of the secondary growth membrane (Figure 3.6) reveal a continuous layer of uniform-sized MOF-5 crystals with an approximate thickness of 14 μm. The single crystals are much smaller (≤ 15 μm) than the as-synthesized crystals. This is a result of grinding the crystals that were used in the seed suspension. Small, uniform crystals are desired for the synthesis of a continuous membrane layer. Even though a continuous seed layer is observed, intercrystalline gaps and defects are observed, evidencing the lack of crystal intergrowth. The XRD pattern of this membrane (Figure 3.7) shows that the crystals grown are MOF-5. The position and intensity of the main peaks match well with those of the XRD pattern of the crystals prepared in this work, and with the MOF-5 membranes prepared by secondary growth method by Huang et al. (2003) and Yoo et al. (2009). Comparing the XRD pattern of this membrane with the pattern of the crystals, no apparent preferred orientation is observed on the membrane.

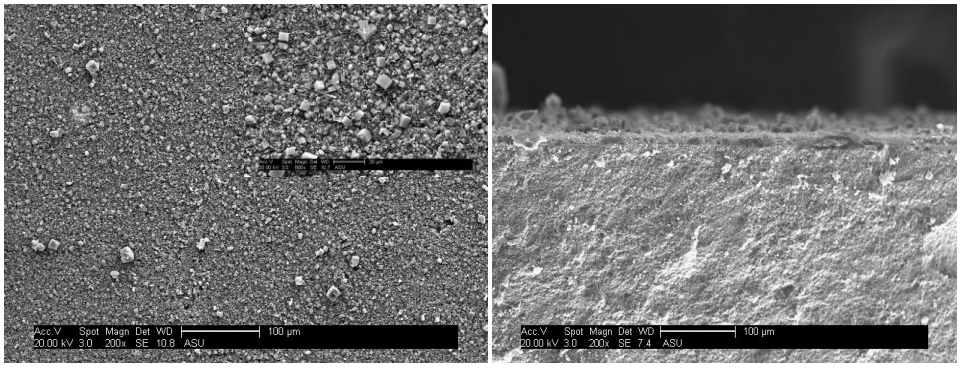

Figure 3.6. SEM image of the surface and the cross-sectional view of a MOF-5 membrane synthesized by secondary growth method. The inset shows an enlarged view.

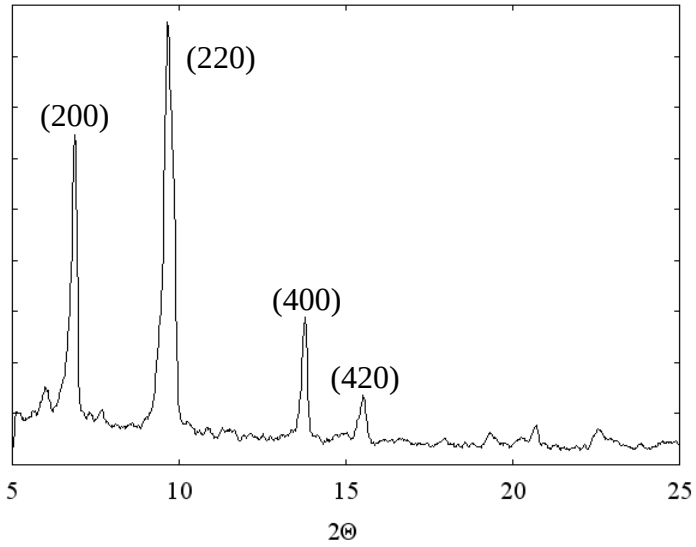

Figure 3.7. XRD pattern of MOF-5 membrane synthesized by secondary growth method.

SEM and XRD of a MOF-5 membrane synthesized by the in situ method used by Liu et al. (2009) are shown in Figures 3.8 and 3.9. SEM surface and cross-section images show a layer of MOF-5 crystals randomly grown on the support surface with a thickness of about 16 μm. Although it seems that the support surface was completely covered, the seeds are not closely packed because of their non-uniform size, and intercrystalline gaps could not be filled. The XRD pattern matches with the pattern for MOF-5 crystals, indicating that the structure obtained was that of MOF-5. The SEM and XRD pattern is similar to those presented by Liu et al., although the peak at 6.9 ° has lower intensity and the peak at 9.7° is split into two. The change in relative peak intensity and the peak splitting are explained by the crystallographic studies done by Hafizovic et al. (2007). Under different synthesis conditions the MOF-5 lattice cell is slightly

distorted and the symmetry changes from cubic (Fm-3m) to rhombohedral structure (R-3m).

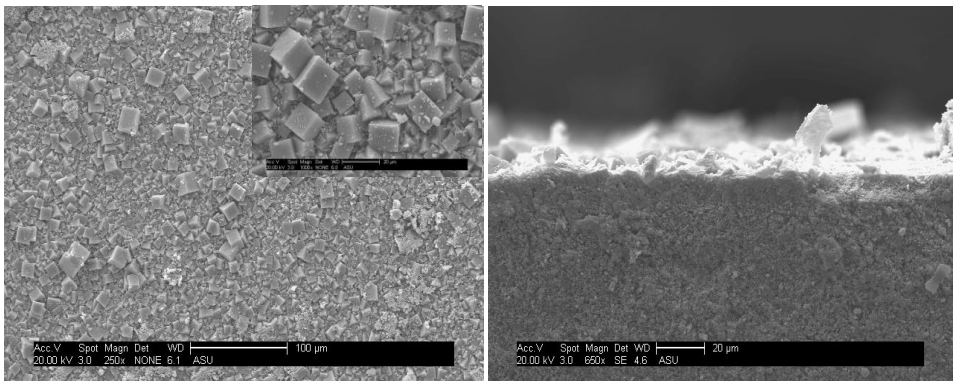

Figure 3.8. SEM image of the surface and the cross-sectional view of a MOF-5 membrane synthesized by in situ method. The inset shows an enlarged view.

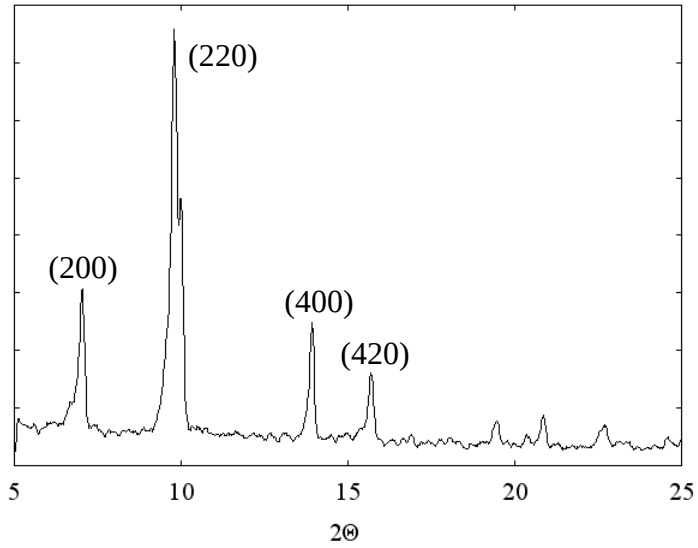

Figure 3.9. XRD pattern of MOF-5 membrane synthesized by in situ method.

The crystal size of the secondary growth membrane is smaller and more uniform than the size of the crystals of in situ membrane. The in situ membrane is slightly thicker than the secondary growth membrane. The first peak of the XRD pattern of this membrane has less intensity than the first peak of the secondary

growth membrane pattern. Also, the second peak is split into two peaks, which indicates that the in situ membrane has a lattice cell distortion.

3.3.3 Gas permeation of MOF-5 membranes. The permeance of both membranes was measured using Helium (He) and Nitrogen (N_2) as single gases. The permeation results for the secondary growth membrane are shown in Figure 3.10. He permeance through the support was measured before and after coating with MOF-5 seeds followed by N_2 permeance measurements through the composite membrane. Table 3.1 summarizes the values of coefficients α, β and β/α obtained from a regression analysis of permeance as function of average pressure. Permeance reduction of He is observed after the MOF-5 layer is grown, with a slight increase with average pressure. This is indicated by the decrease of values of α before (1.31×10^{-6} mol m^{-2} Pa^{-1} s^{-1}) and after the MOF-5 coating (1.20×10^{-6} mol m^{-2} Pa^{-1} s^{-1}). However, the values of β increased from 3.54×10^{-13} mol m^{-2} Pa^{-2} s^{-1} to 6.08×10^{-13} mol m^{-2} Pa^{-2} s^{-1}, increasing the β/α ratio after coating. Since this ratio is a measure of the average pore size of the membrane, an increase of β, and β/α after coating the MOF-5 layer suggests the presence of defects. N_2 permeance through the composite membrane was lower than He permeance, indicating Knudsen diffusion behavior (i.e. the permeance is proportional to $Mwt^{-1/2}$). However, the experimental permeance ratio of He to N_2 (2.46) was lower than the theoretical ratio (2.64). This is due to the viscous flow through the defects in the membrane layer. In an attempt to repair the defects, a second step of secondary growth was done on the defective membrane. However, as indicated by the increase in β/α ratio, the defects were not repaired. The contribution of the

membrane defects is evident by the increased slope of the calculated permeance for the membrane layer.

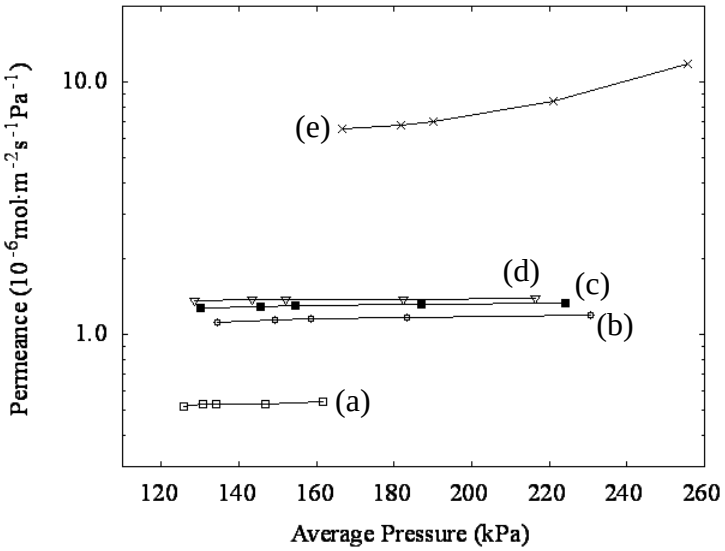

Figure 3.10. Permeance through secondary growth membrane as function of average pressure: (a) nitrogen through composite membrane, (b) helium through composite membrane after 2 secondary growth steps, (c) helium through composite membrane after 1 secondary growth step, (d) helium through alumna support, (e) helium through membrane layer (calculated).

Table 3.1

Summary of intercept α, slope β and β/α through secondary growth membrane

	Gas	Intercept, α	Slope, β	β/α
Support	He	1.31×10^{-6}	3.54×10^{-13}	2.69×10^{-7}
Comp. memb. (1 s.g)	He	1.20×10^{-6}	6.08×10^{-13}	5.05×10^{-7}
Comp. memb. (2 s.g)	He	1.02×10^{-6}	7.50×10^{-13}	7.29×10^{-7}
Comp. memb. (1s.g.)	N_2	4.65×10^{-7}	4.65×10^{-13}	1.02×10^{-6}
Memb. layer	He	4.14×10^{-6}	6.02×10^{-11}	1.45×10^{-5}

Using the same conditions as tested with the secondary growth membrane, permeance measurements were done with the in situ membrane, and the results are shown in Figure 3.11. Table 3.2 shows a summary of the coefficients α, β and β/α obtained from the regression analysis. Similar to the secondary growth membrane, the in situ membrane had a decrease in He permeance after the MOF-5 layer was coated on the support surface. N_2 permeance was even lower than the He permeance through the composite membrane, showing Knudsen diffusion behavior. Coefficient α decreased with the composite membrane, but β increased. Again, this caused an increase in the β/α ratio from 3.91 x 10^{-7} Pa^{-1} to 6.55 x 10^{-7} Pa^{-1}, therefore the average pore size increased. Although the experimental permeance ratio of He to N_2 (2.65) was almost the same as the theoretical ratio, indicating a strong Knudsen flow behavior, the increase in average pore size indicates that the membrane has defects that contribute viscous flow behavior. The permeance of the membrane layer is in the same order of magnitude of the permeance reported by the continuous MOF-5 membrane prepared by a similar in situ procedure by Liu et al. (2009), but decreases with average pressure. It is possible that the permeance area changed due to compression of the O-rings used to seal the membrane in the membrane cell.

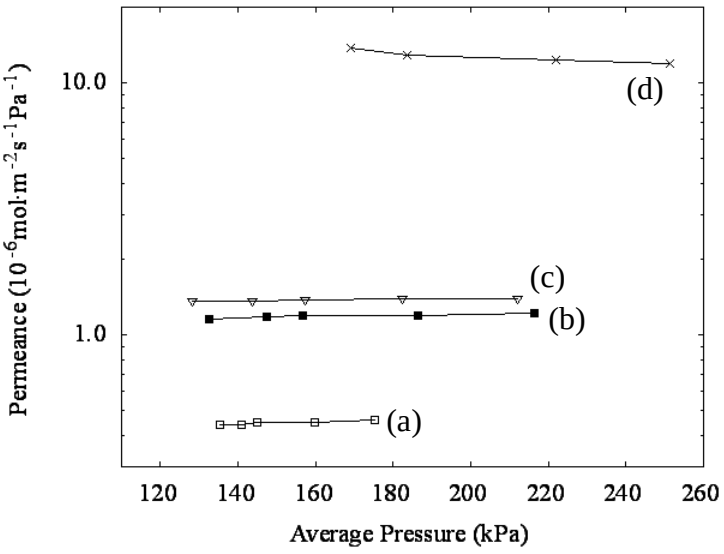

Figure 3.11. Permeance through in situ membrane as function of average pressure: (a) nitrogen through composite membrane, (b) helium through composite membrane, (c) helium through alumna support, (d) helium through membrane layer (calculated).

Table 3.2

Summary of intercept α, slope β and β/α through in situ membrane

	Gas	Intercept, α	Slope, β	β/α
Support	He	1.29×10^{-6}	5.05×10^{-13}	3.91×10^{-7}
Comp. memb.	He	1.07×10^{-6}	7.01×10^{-13}	6.55×10^{-7}
Comp. memb.	N_2	3.67×10^{-7}	5.35×10^{-13}	1.45×10^{-6}
Memb. layer	He	1.68×10^{-5}	-1.97×10^{-11}	-1.17×10^{-6}

These results show that the gas permeation of He and N_2 through both membranes is determined by a combination of Knudsen diffusion and viscous flow. The latter one indicates that the membranes have defects.

3.4 Conclusions

MOF-5 membranes were synthesized by secondary growth and in situ methods. Characterization by XRD and SEM show that MOF-5 layers with a thickness of 14-16 μm were grown on α-alumina supports by both synthesis methods. The XRD pattern of the in situ membrane indicates that it may have a small crystal distortion due to framework interpenetration. As shown by SEM, this membrane also has larger and non-uniform crystal size. Single gas permeation results indicate that gas transport through both membranes can be described by Knudsen diffusion and viscous flow. The contribution of viscous flow indicates that the membranes have defects. To further investigate the performance of both membranes, gas permeation experiments with a mixture of gases needs to be conducted.

Chapter 4

SUMMARY AND RECOMMENDATIONS

4.1 Summary

This thesis presents early work on two approaches to separate and capture CO_2: adsorption on solid sorbents and membrane separation. A brief background of CO_2 separation and capture methods, and of these two approaches is given in Chapter 1. Current amine absorption processes used in industry are mature, but have large room for improvement. Amine modified aerogels and MOF-5 membranes are promising methods to achieve significant reductions on CO_2 emissions in a cost-effective manner.

In Chapter 2, synthesis of amine functionalized aerogels by physical adsorption, MAIC and ALD methods is studied. CO_2 adsorption uptake of the sorbents is measured in a microbalance. Hydrodynamic characteristics of aerogels in a fluidized bed are also studied. Sorbents prepared by physical adsorption had the highest CO_2 capture capacity (1.43-1.63 mmol CO_2/g). These are followed by a sorbent made by doing ALD on hydrophilic aerogels at atmospheric pressures with a CO_2 capactiy of 1.23 mmol/g. For all these experiments, no water vapor was added to the gas stream. Unfortunately, the CO_2 adsorption capacity of these sorbents is not high enough to replace current separation and capture technology. Hydrophobic aerogels fluidized better than hydrophilic aerogels, due to the stronger interparticle forces caused by liquid bridges present in the latter. Duomeen modified aerogels appeared to be heavily agglomerated and did not

fluidize even with the assistance of a micro-jet at the operating conditions used in the experiments.

Chapter 3 reports the synthesis and characterization of MOF-5 membranes synthesized by secondary growth and in situ methods. SEM and XRD characterization confirmed the growth of MOF-5 membranes by both synthesis methods. Single gas permeance results showed Knudsen diffusion and viscous flow transport behavior, indicating that both membranes have defects.

4.2 Recommendation

Based on the experimental studies done in this work, the following recommendations are suggested for future study of the amine modified aerogels:

1. Conduct a systematic study to test different amines and different aerogels to achieve maximum amine loading on the aerogels, and maximum CO_2 adsorption capacity.

2. Repeat ALD at atmospheric pressures, but with hydrophobic aerogels to minimize water vapor adsorption by the sorbent.

3. Measure CO_2 adsorption capacity at higher temperatures.

4. Study the role of water in the reaction between CO_2 and amines.

5. Use higher superficial gas velocities through the distributor or smaller nozzle size for the microjet to successfully to fluidize the amine modified powder.

The recommendations suggested for future study of MOF-5 membranes are:

1. Study optimal synthesis and experimental conditions to minimize membrane defects

2. Conduct gas permeation experiments at high pressures and temperatures to measure permeance and selectivity of MOF-5 membranes on a binary gas mixture containing CO_2.

3. Do amine functionalization on MOF-5 membrane to enhance CO_2 selectivity

REFERENCES

Akimov, Y. K. (2003). Fields of application of aerogels (review). *Pribory i Tekhnika Eksperimenta, 46*(3), 5-19.

Arruebo, M., Mallada, R., & Pina, M. P. (2009). Chapter 10. zeolite membranes: Synthesis, characterization, important applications, and recent advances. In A. K. Pabby, S. S. H. Rizvi & A. M. Sastre (Eds.), *Handbook of membrane separations* (pp. 270-274). Florida, USA: Taylor and Francis Group, LLC.

Ata, A., Rabinovich, Y. I., Singh, R. K., & Hendrickson, W. (1998). *Material Research Society Symposium Proceedings, 501*.

Barron, A.*Atomic layer deposition.* Retrieved July 13, 2009, from http://cnx.org/content/m25737/1.2/

Baumann, T. F., Biener, J., Wang, Y. M., Kucheyev, S. O., Nelson, E. J., Satcher, J. H., Elam, J. W., Pellin, M. J., & Hamza, A. V. (2006). Atomic layer deposition of uniform of uniform metal coatings on highly porous aerogel substrates. *Chemistry of Materials, 18*, 6106-6108.

Cabot Corporation. (2003). *Nanogel^{TM}: Fine particle aerogel.* Retrieved 5/10, 2009, from www.cabot-corp.com/nanogel

Drage, T. C., Arenillas, A., Smith, K. M., & Snape, C. E. (2008). Thermal stability of polyethylenimine based carbon dioxide adsorbents and its influence on selection of regeneration strategies. *Microporous Mesoporous Materials, 116*(1-3), 504-512.

Ferguson, J. D., Weimer, A. W., & George, S. M. (2002). Atomic layer deposition of boron nitride using sequential exposures of BCl_3 and NH_3. *Thin Solid Films, 413*, 16-25.

Gascon, J., & Kapteijn, F. (2010). Metal-organic membranes - high potential, bright future? *Angewandte Chemie International Edition, 49*, 2-5.

Geldart, D. (1990). Chapter 6. Gas fluidization. In M. Rhodes (Ed.), *Principles of powder technology* (First ed., pp. 119-142). New York, USA: John Wiley & Sons Ltd.

Ghosal, S., Baumann, T. F., King, J. S., Kucheyev, S. O., Wang, Y. M., Worsley, M. A., Biener, J., Bent, S. F., & Hamza, A. V. (2009). Controlling atomic layer deposition of TiO_2 in aerogel through surface functionalization. *Chemistry of Materials, 21*, 1989-1992.

Gray, M. L., Champagne, K. J., Fauth, D., Baltrus, J. P., & Pennline, H. (2008). Performance of immobilized tertiary amine solid sorbents for the capture of carbon dioxide. *International Journal of Greenhouse Gas Control, 2*, 3-8.

Hafizovic, J., Bjorgen, M., Olsbye, U., Dietzel, P. D. C., Bordiga, S., Prestipino, C., Lamberti, C., & Lillerud, K. P. (2007). The inconsistency in adsorption properties and powder XRD data of MOF-5 is rationalized by framework interpenetration and the presence of organic and inorganic species in the nanocavities. *Journal of American Chemical Society, 129*, 3612-3620.

Hakim, L. F., George, S. M., & Weiner, A. W. (2005). Conformal nanocoating of zirconia nanoparticles by atomic layer deposition in a fluidized bed reactor. *Nanotechnology, 16*, S375-S381.

Hermes, S., Zacher, D., Baunemann, A., Woll, C., & Fischer, R. A. (2007). Selective growth and MOCVD loading of small single crystals of MOF-5 at alumina and silica surfaces modified with organic self-assembled monolayers. *Chemistry of Materials, 19*, 2168-2173.

Hiyoshi, N., Yogo, K., & Yashima, T. (2004). Adsorption of carbon dioxide on amine modified SBA-15 in the presence of water vapor. *Chemistry Letters, 33*, 510.

Hook, R. J. (1997). An investigation of some sterically hindered amines as potential carbon dioxide scrubbing compounds. *Industrial & Engineering Chemistry Research, 36*, 1779-1790.

Huang, H. Y., Yang, R. t., Chinn, D., & Munson, C. L. (2003). Amine-grafted MCM-48 and silica xerogel as superior sorbents for acidic gas removal from natural gas. *Industrial & Engineering Chemistry Research, 42*, 2427.

Huang, L., Wang, H., Chen, J., Wang, Z., Sun, J., Zhao, D., & Yan, Y. (2003). Synthesis, morphology control, and properties of porous metal-organic coordination polymers. *Microporous and Mesoporous Materials, 58*, 105-114.

Hunt, A., & Ayers, M. R. (2004). *Silica aerogels.* Retrieved November, 2008, from http://eetd.lbl.gov/ecs/aerogels/sa-chemistry.html

Hüsing, N., & Schubert, U. (1998). Aerogels - airy materials: Chemistry, structure and properties. *Angewandte Chemie International Edition, 37*(1-2), 22-45.

Jayaraman, V., & Lin, Y. S. (1995). Synthesis and hydrogen permeation properties of ultra-thin palladium-silver alloy membranes. *Journal of Membrane Science, 104*, 251-262.

Kucheyev, S. O., Biener, J., Wang, Y. M., Brauman, T. F., Wu, K. J., van Burren, T., Hamza, A. V., Satcher, J. M., Elam, J. W., & Pellin, M. J. (2005). Atomic layer deposition of ZnO on ultralow-density nanoporous silica aerogel monoliths. *Applied Physics Letters, 86*, 083108-1.

Kunii, D., & Levenspiel, O. (1991). The Geldart classification of particles. In *Fluidization engineering* (Second ed., pp. 77). Massachusetts, USA: Butterworth-Heinemann.

Leal, O., Bolivar, C., Ovalles, C., Garcia, J. J., & Espidel, Y. (1995). Reversible adsorption of carbon dioxide on amine surface-bonded silica gel. *Inorganica Chimica Acta, 240*, 183-189.

Li, H., Eddaoudi, M., O'Keeffe, M., & Yaghi, O. M. (1999). Design and synthesis of an exceptionally stable and highly porous metal-organic framework. *Nature, 402*, 276-279.

Lin, J. Y. S., Kumakiri, I., Nair, B. N., & Alsyouri, H. (2002). Microporous inorganic membranes. *Separation and Purification Methods, 31*(2), 229-379.

Liu, Y., Ng, Z., Khan, E. A., Jeong, H. -., Ching, C. -., & Lai, Z. (2009). Synthesis of continuous MOF-5 membranes on porous α-alumina substrates. *Microporous and Mesoporous Materials, 118*, 296-301.

Mallada, R., & and Menéndez, M. (2008). Chapter 5. Preparation and characterization of zeolite membranes. In *Inorganic membranes: Synthesis, characterization and applications* (First ed., pp. 135-146). Amsterdam, The Netherlands: Elsevier B.V.

O'Brien, J. (2009). *A study of the microstructure-property relationship for MFI-type zeolite membranes for xylene separation.* (Doctorate, Arizona State University).

Panella, B., Hirscher, M., Putter, H., & Muller, U. (2006). Hydrogen adsorption in metal-organic frameworks: Cu-MOFs and Zn-MOFs compared. *Advanced Functional Materials, 16*, 520-524.

Pfeffer, R., Quevedo, J. A., & Flesch, J. (2007). *Fluidization system enhanced by micro-jet flow*. US Patent Application No. 9435000032, Washington, DC: US Patent and Trademark Office

Quevedo, J. A., Omosebi, A., & Pfeffer, R. (2010). Fluidization enhancement of agglomerates of metal-oxide nano-powders by micro-jets. *AIChE Journal, 56*(6), 1456-1468.

Ramlakhan, M., Wu, C., Watano, S., Dave, R. N., & Pfeffer, R. (2000). Dry particle coating using magnetically assisted impaction coating (MAIC): Modification of surface properties and optimization of system and operating parameters. *Powder Technology, 112*(1-2), 137-148.

Ranjan, R., & Tsapatsis, M. (2009). Microporous metal organic membrane on porous support using seeded growth method. *Chemistry of Materials, 21*, 4920-4924.

Rinker, E. B., Ashour, S. S., & Sandall, O. C. (2000). Absorption of carbon dioxide into aqueous blends of diethanolamine and methyldiethanolamine. *Industrial & Engineering Chemistry Research, 39*(11), 4346-4356.

Ritala, M., & Leskela, M. (2002). Chapter 2. Atomic layer depositon. In M. S. Nalwa (Ed.), *Handbook of thin film materials* (Vol. 1 ed., pp. 103-159) Academic Press.

Sanz, R., Calleja, G., Arencibia, A., & Sanz-Pérez, E. S. (2010). Carbon dioxide adsorption on branched polyetheleneimine-impregnated mesoporous silica SBA-15. *Applied Surface Science, 256*, 5323-5328.

Serna-Guerrero, R., Da'na, E., & Sayari, A. (2008). New insights into the interactions of carbon dioxide with amine-functionalized silica. *Industrial & Engineering Chemistry Research, 47*, 9406-9412.

Tsao, C.S., Yu, M.S., Chung, T.Y., Wu, H.C.; Wang, C.Y., Chang, K.S., & Chen, H.L. (2007). Characterization of pore structure in metal-organic framework by small-angle X-ray scattering. *Journal of American Chemical Society, 129*, 15997-16004.

Xu, X., Song, C., Andresen, J. M., Miller, B. G., & Scaroni, A. W. (2002). Novel polyetheleneimine-modified mesoporous molecular sieve of MCM-41 type as high-capacity adsorbent for carbon dioxide capture. *Energy and Fuels, 16*, 1463-1469.

Yaghi, O. M., O'Keefe, M., Ockwig, N. W., Chae, H. K., Eddaudi, M., & Kiril, J. (2003). Reticular synthesis and the doping of new materials. *Nature, 423*, 705-714.

Yang, H., Xu, Z., Fan, M., Gupta, R., Slimane, R. B., Bland, A. E., & Wright, I. (2008). Progress in carbon dioxide separation and capture: A review. *Journal of Environmental Sciences, 20*, 14-27.

Yang, Y., Silva, A., Banerje, A., Dave, R. N., & Pfeffer, R. (2005). Dry particle coating for improving the flowability of cohesive powders. *Powder Technology, 158*, 21-33.

Yoo, Y., Lai, Z., & Jeong, H.K. (2009). Fabrication of MOF-5 membranes using microwave-induced rapid seeding and solvothermal secondary growth. *Microporous Mesoporous Materials, 21*, 4920-4924.

Zhao, Z., Li, Z., & Lin, Y. S. (2009). Adsorption and diffusion of carbon dioxide on metal-organic framework (MOF-5). *Industrial & Engineering Chemistry Research, 48*, 10015-10020.

Zhu, C., Yu, Q., Pfeffer, R., & Dave, R. N. (2005). Gas fluidization characteristics of nanoparticle agglomerates. *AICHE Journal*, *51*(2), 426-439.

APPENDIX A

EXPERIMENTAL PROCEDURES FOR MOF-5 MEMBRANES

A1. Preparation of alumina supports

Homemade porous α-alumina supports, with thickness of 2mm and diameter of 20mm were prepared by the following method:

1. Weigh 22 g of alumina powder (A16 SG, Alcoa) and add 12 wt% of distilled water.

2. Mix water and powder with mortar and pestle by adding the water in small amounts. Mix until mixture becomes a homogeneous fine powder. Keep mixture covered to avoid evaporation of water.

3. Measure 2.1 g of the mixture in a stainless steel support mold and shake mold to evenly distribute powder.

4. In a pressing machine (Carver, Inc.) press sample to 5000 psi for 2 minutes. Then press to 20000 psi for 5 minutes. Increase the pressure slowly.

5. Flip mold, remove pressed disk and place it in a Petri dish. Keep disk in oven at 40 °C and 60% relative humidity.

6. Place supports on ceramic porous plate and sinter them in a high temperature sintering furnace. Use the following temperature program:

Table A.1

Temperature Program for Sintering Supports

Step	Ramp Rate (°C/hr)	Temperature (°C)	Hold Time (hr)
1	60	600	0.1
2	96	1260	0.1
3	96	200	0.1
4	60	1150	30
5	60	200	0.1
6	---	---	End

7. Polish one face of the supports using polisher (Metaserv 2000) at approximately 400 rpm with polishing paper #500, #800 and #1200 (Silicon Carbide). Polish with each paper for about 10 minutes, or until disk surface is smooth.

8. Dry supports at 60°C overnight.

A.2 Preparation of MOF-5 crystals

MOF-5 crystals and membranes were synthesized starting from terephthalic acid (BDC), zinc nitrate hexahydrate ($Zn(NO_3)_2 \cdot 6H_2O$) and N, N-dimethylformamide (DMF) as the organic solvent. All chemicals were purchased from Fluka, and are of the highest grades available (99+ %). The synthesis procedure is as follows:

1. Weigh 1.664 g of zinc nitrate and 0.352g of BDC and dissolved in 40 mL of degassed DMF solvent. Transfer solution to a glass vial and seal with a cap.

2. In an oil bath at 130 °C, heat solution in glass vial for 4 hours by hydrothermal synthesis and under autogenous pressure.

3. After synthesis completion, remove glass vial from oil bath and allow cooling to room temperature. Open cap before crystals are completely cools down.

4. Filter off crystals and wash 3 times with fresh DMF solvent.

5. Immerse crystals in chloroform and place in oven at 70 °C for 2 days. Replenish chloroform every day.

6. Dry crystals overnight in vacuum oven at 80 °C.

7. Store crystals in desiccator while not in use.

A.3 Preparation of crystal suspension and dip coating

A.3.1Crystal suspension

1. Grind synthesized MOF-5 crystals in ball-mill type mixer with Zirconia balls for up to 12 hours.

2. Weigh 0.15 g of ground powder and mix with 9.8 g of DMF.

3. Stir in hot plate stirrer at room temperature for 3 hours.

A.3.2 Dip coating

1. Wash polished support with ethanol and deionized water in ultrasonic bath for 10 minutes. Dry supports at 120 °C for 24 hours.

2. Immerse polished face of support in the stable suspension, holding it with tweezers for 3-6 seconds.

3. Remove disk from the suspension and clean excess liquid from the edges.

4. Dry support in oven at 50 °C for 24 hours.

5. Repeat dip coating one more time.

A.4 Synthesis of MOF-5 membranes by secondary growth method

1. Weigh 0.832 g of zinc nitrate and 0.176 g of BDC and dissolve in 40 mL of DMF.

2. Slowly add 0.137 g of N-ethyldiisopropylamine (EDIPA) (~5 drops) under vigorous stirring to help initiating the coordination.

3. Immerse support, held with Teflon holder, into the solution, and seal.

4. Heat in oil bath to 130 °C for 4 hours by hydrothermal synthesis and autogeneous pressure.

5. After 4 hours remove vial from oil bath and allow cooling down to room temperature.

6. Remove membranes and washed with DMF solution 3 times.

7. Immerse membranes in chloroform for 2 days, replenishing with fresh chloroform every day.

8. Dry membranes overnight in vacuum oven at 80 °C. Keep membrane in vacuum oven.

A.5 Synthesis of MOF-5 membranes by in situ method

A continuous MOF-5 membrane was synthesized by following the procedure detailed in (Liu et al., 2009).

1. Dehydrate zinc nitrate at 80 °C under vacuum for 12 hours.

2. Dissolve 0.063 g of BDC in 10 mL of DMF and load in Teflon-lined autoclave.

3. Immerse support in solution for 30 minutes with polished surface facing up.

4. Add 0.340 g of dehydrated zinc nitrate.

5. Seal autoclave and heat in oven to 105 °C for 24 hours.

6. After completion of the synthesis, remove autoclave from oven and allow cooling down to room temperature.

7. Decant solvent and wash membrane with fresh DMF.

8. Immerse membrane in chloroform for 12 hours.

9. Dry membrane under vacuum at 60 °C for 24 hours.

APPENDIX B

EXPERIMENTAL PROCEDURES TO MODIFY AEROGELS

B.1 Physical adsorption of Duomeen T and Triameen T

1. Weigh 7.5 g of Duomeen T or Triameen T surfactant and add to 150 mL of distilled water.

2. Mix in ball-mill type mixer overnight to dissolve surfactant in water.

3. Add 5 g of aerogels (size range 65-100 μm), and mix in ball-mill mixer overnight or until aerogels no longer float on top of the solution.

4. Filter resulting slurry, and dry at 100 °C.